J|A|C|S
ARTICLES
Published on Web 04/02/2004

Bimetallic Cluster Complexes: The Synthesis, Structures, and Bonding of Ruthenium Carbonyl Cluster Complexes Containing Palladium and Platinum with the Bulky Tri-*tert*-butyl-phosphine Ligand

Richard D. Adams,*,† Burjor Captain,† Wei Fu,† Michael B. Hall,‡ Josiah Manson,‡ Mark D. Smith,† and Charles Edwin Webster‡

Contribution from the Department of Chemistry and Biochemistry and the USC NanoCenter, University of South Carolina, Columbia, South Carolina 29208, and Department of Chemistry, Texas A&M University, College Station, Texas 77843-3255

Received November 11, 2003; E-mail: adams@mail.chem.sc.edu

Abstract: The bis-phosphine compounds $M(PBu^t_3)_2$, M = Pd and Pt, readily eliminate one PBu^t_3 ligand and transfer $MPBu^t_3$ groups to the ruthenium−ruthenium bonds in the compounds $Ru_3(CO)_{12}$, $Ru_6(CO)_{17}$-(μ_6-C), and $Ru_6(CO)_{14}(\eta^6\text{-}C_6H_6)(\mu_6\text{-C})$ without displacement of any of the ligands on the ruthenium complexes. The new compounds, $Ru_3(CO)_{12}[Pd(PBu^t_3)]_3$, **10**, and $Ru_6(CO)_{17}(\mu_6\text{-C})[Pd(PBu^t_3)]_2$, **11**, $Ru_6(CO)_{17}(\mu_6\text{-C})$-$[Pt(PBu^t_3)]_n$, $n = 1$ (**12**), $n = 2$ (**13**), and $Ru_6(CO)_{14}(\eta^6\text{-}C_6H_6)(\mu_6\text{-C})[Pd(PBu^t_3)]_n$, $n = 1$ (**15**), $n = 2$ (**16**), have been prepared and structurally characterized. In most cases the $MPBu^t_3$ groups bridge a pair of mutually bonded ruthenium atoms, and the associated Ru−Ru bond distance increases in length. Fenske−Hall calculations were performed on **10** and **11** to develop an understanding of the electron deficient metal−metal bonding. **10** undergoes a Jahn−Teller distortion to increase bonding interactions between neighboring $Ru(CO)_4$ and $Pd(PBu^t_3)$ fragments. **11** has seven molecular orbitals important to cluster bonding in accord with cluster electron-counting rules.

Introduction

Heteronuclear (mixed-metal) cluster complexes have been shown to be good precursors for the preparation of supported bimetallic nanoparticles.[1−8] On supports these nanoparticles have proven to be highly active catalysts.[9,10] Palladium−ruthenium and platinum−ruthenium clusters supported on mesoporous silica have been shown to exhibit high activity for catalytic hydrogenation reactions.[9,10]

Significant advances have been made in the systematics of the syntheses of heteronuclear metal cluster complexes over the past 20 years.[11] Bridging ligands derived from the main group elements are widely used as agents for the aggregation and stabilization of metal clusters.[12]

We have recently shown that the bis-phosphine compounds $M(PBu^t_3)_2$, M = Pd and Pt, are excellent reagents for the transfer $MPBu^t_3$ groups to ruthenium−ruthenium and ruthenium−platinum bonds to yield a variety of new heteronuclear cluster complexes that employ delocalized bonding schemes.[13] For example, we have recently reported the complex $Ru_5(CO)_{15}$-(C)[$PtPBu^t_3$], **1**, formed by the addition of a $Pt(PBu^t_3)$ group to the square-pyramidal pentaruthenium cluster complex Ru_5-$(CO)_{15}(\mu_5\text{-C})$. Interestingly, compound **1** exists in solution as a

† University of South Carolina.
‡ Texas A&M University.

(1) Toshima, N.; Yonezawa, T. *New J. Chem.* **1998**, 1179.
(2) Johnson, B. F. G. *Coord. Chem. Rev.* **1999**, *192*, 1269.
(3) Midgley, P. A.; Weyland, M.; Thomas, J. M.; Johnson, B. F. G. *Chem. Commun.* **2001**, 907.
(4) Nashner, M. S.; Frenkel, A. I.; Somerville, D.; Hills, C. W.; Shapley, J. R.; Nuzzo, R. G. *J. Am. Chem. Soc.* **1998**, *120*, 8093.
(5) Nashner, M. S.; Frenkel, A. I.; Adler, D. L.; Shapley, J. R.; Nuzzo, R. G. *J. Am. Chem. Soc.* **1997**, *119*, 7760.
(6) Shephard, D. S.; Maschmeyer, T.; Johnson, B. F. G.; Thomas, J. M.; Sankar, G.; Ozkaya, D.; Zhou, W.; Oldroyd, R. D.; Bell, R. G. *Angew. Chem., Int. Ed. Engl.* **1997**, *36*, 2242.
(7) Raja, R.; Sankar, G.; Hermans, S.; Shephard, D. S.; Bromley, S.; Thomas, J. M.; Johnson, B. F. G. *Chem. Commun.* **1999**, 1571.
(8) Shephard, D. S.; Maschmeyer, T.; Sankar, G.; Thomas, J. M.; Ozkaya, D.; Johnson, B. F. G.; Raja, R.; Oldroyd, R. D.; Bell, R. G. *Chem. Eur. J.* **1998**, *4*, 1214.
(9) (a) Thomas, J. M.; Johnson, B. F. G.; Raja, R.; Sankar, G.; Midgley, P. A. *Acc. Chem. Res.* **2003,** *36*, 20. (b) Braunstein, P.; Rose, J. In *Catalysis by Di- and Polynuclear Metal Cluster Complexes*; Adams, R. D., Cotton, F. A., Eds.; VCH: New York, 1998; Chapter 13, p 443.
(10) (a) Raja, R.; Khimyak, T.; Thomas, J. M.; Hermans, S.; Johnson, B. F. G. *Angew. Chem., Int. Ed.* **2001**, *40*, 4638. (b) Hermans, S.; Raja, R.; Thomas, J. M.; Johnson, B. F. G.; Sankar, G.; Gleeson, D. *Angew. Chem., Int. Ed.* **2001**, *40*, 1211. (c) Raja, R.; Sankar, G.; Hermans, S.; Shephard, D. S.; Bromley, S.; Thomas, J. M.; Johnson, B. F. G.; Maschemeyer, T. *Chem. Commun.* **1999**, 1571.
(11) (a) Adams, R. D. In *Comprehensive Organometallic Chemistry II*; Abel, E. W., Stone, F. G. A., Wilkinson, G., Eds.; Pergamon: Oxford, 1995; Vol. 10, p 1. (b) Adams, R. D. In *The Chemistry of Metal Cluster Complexes*; Shriver, H. D., Kaesz, H. D., Adams, R. D., Eds.; VCH: New York, 1990; Chapter 3, p 121. (c) Roberts, D. A.; Geoffroy, G. L. In *Comprehensive Organometallic Chemistry*; Wilkinson, G., Stone, F. G. A., Abel, E. W., Eds.; Pergamon: Oxford, 1982; Vol. 6, Chapter 40, p 763.
(12) (a) Hidai, M.; Kuwata, S.; Mizobe, Y. *Acc. Chem. Res.* **2000**, *33*, 46. (b) Whitmire, K. H. *Adv. Organomet. Chem.* **1998**, *42*, 1. (c) Audi Fong, S.-W.; Hor, T. S. A. *J. Chem. Soc., Dalton Trans.* **1999**, 639. (d) Shibihara, T. *Coord. Chem. Rev.* **1993**, *123*, 73. (e) Whitmire, K. H. *J. Coord. Chem.* **1988**, *17*, 95. (f) Adams, R. D.; Tasi, M. *J. Cluster Sci.* **1990**, *1*, 249.
(13) (a) Adams, R. D.; Captain, B.; Fu, W.; Smith, M. D. *J. Am. Chem. Soc.* **2002**, *124*, 5628. (b) Adams, R. D.; Captain, B.; Fu, W.; Pellechia, P. J.; Smith, M. D. *Angew. Chem., Int. Ed.* **2002**, *41*, 1951. (c) Adams, R. D.; Captain, B.; Fu, W.; Pellechia, P. J.; Smith, M. D. *Inorg. Chem.* **2003**, *42*, 2094. (d) Adams, R. D.; Captain, B.; Fu, W.; Smith, M. D. *J. Organomet. Chem.* **2003**, *682*, 113.

mixture of open and closed isomers **1a** and **1b** that are in rapid equilibrium on the NMR time scale at room temperature. The palladium compounds $Ru_5(CO)_{15}(\mu_6\text{-}C)[Pd(PBu^t_3)]_n$, where $n = 1$ (**2**), $n = 2$ (**3**), were also prepared and engaged in similar dynamical processes.[13b,c] We have shown that $Pt(PBu^t_3)$ and $Pd(PBu^t_3)$ groups add across Ru−Ru bonds as well as Ru−Pt bonds in the mixed-metal complex $PtRu_5(CO)_{16}(\mu_6\text{-}C)$ to afford the adducts $PtRu_5(CO)_{16}(\mu_6\text{-}C)[M(PBu^t_3)]_n$, **4** and **5**, where M = Pt and $n = 1$ or $n = 2$, respectively, and **6** and **7,** where M = Pd and $n = 1$ or $n = 2$, respectively.[13d]

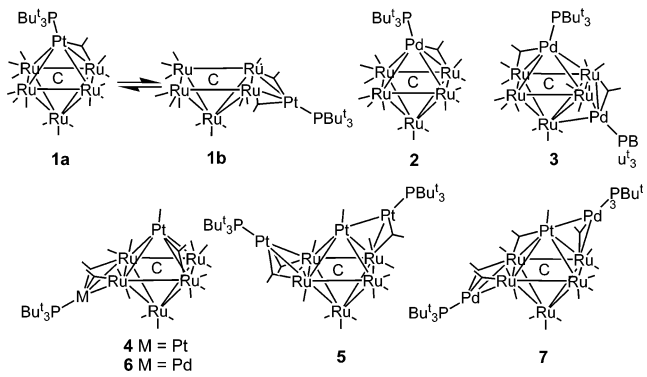

In a recent communication we described the reactions of $Ru_3(CO)_{12}$, **8**, and $Ru_6(CO)_{17}(\mu_6\text{-}C)$, **9**,[14] with $Pd(PBu^t_3)_2$ which yielded the complexes $Ru_3(CO)_{12}[Pd(PBu^t_3)]_3$, **10**, and $Ru_6(CO)_{17}(\mu_6\text{-}C)[Pd(PBu^t_3)]_2$, **11**, respectively, at room temperature. Simple delocalized bonding models were proposed to describe the bonding interactions between the $Pd(PBu^t_3)$ group with the Ru−Ru metal−metal bonds.[13a] The nature of these bonding interactions have now been investigated by molecular orbital calculations. These results along with details of the synthesis and structural analyses of compounds **10**, **11**, $Ru_6(CO)_{17}(\mu_6\text{-}C)[Pt(PBu^t_3)]_n$, where $n = 1$ (**12**), $n = 2$ (**13**), and $Ru_6(CO)_{14}(\eta^6\text{-}C_6H_6)(\mu_6\text{-}C)[Pd(PBu^t_3)]_n$, where $n = 1$ (**15**), $n = 2$ (**16**), are reported herein.

Experimental Section

General Data. All reactions were performed under a nitrogen atmosphere. Reagent grade solvents were dried by the standard procedures and were freshly distilled prior to use. Infrared spectra were recorded on a Nicolet 5DXBO FT-IR or AVATAR 360 FT-IR spectrophotometer. ^1H NMR and ^{31}P NMR were recorded on a Varian Inova 400 spectrometer operating at 399 and 168 MHz, respectively. ^{31}P NMR spectra were externally referenced against 85% *o*-H_3PO_4. Elemental analyses were performed by Desert Analytics (Tucson, AZ). Bis(tri-*tert*-butyl phosphine)palladium(0), $Pd(PBu^t_3)_2$, and $Ru_3(CO)_{12}$, **8**, were purchased from Strem and were used without further purification. $Ru_6(CO)_{17}(\mu_6\text{-}C)$, **9**,[14] $Ru_6(CO)_{14}(\eta^6\text{-}C_6H_6)(\mu_6\text{-}C)$, **14**,[15] and bis(tri-*tert*-butyl phosphine)platinum(0), $Pt(PBu^t_3)_2$[16] were prepared according to the published procedures. Product separations were performed by TLC in air on Analtech 0.25- and 0.5-mm silica gel 60 Å F_{254} glass plates.

Preparation of $Ru_3(CO)_{12}[Pd(PBu^t_3)]_3$, 10. A 10.3 mg amount of **8** (0.016 mmol) dissolved in 15 mL of CH_2Cl_2 was allowed to react with 37.0 mg of $Pd(PBu^t_3)_2$ (0.088 mmol) at 25 °C for 30 min. The solution was concentrated, and 10 mL of hexane was added. Upon cooling to −80 °C, 13.4 mg of blue crystals of $Ru_3(CO)_{12}[Pd(PBu^t_3)]_3$, **10**, precipitated, 49% yield. Spectral data for **10**: IR ν_{CO} (cm^{-1} in CH_2Cl_2): 2056 (m), 2004 (vs), 1984 (s, sh), 1948 (s), 1819 (m). ^1H NMR (in $CDCl_3$): $\delta = 1.43$ ppm (d, 81H, CH_3, $^3J_{P-H} = 12.3$ Hz). $^{31}P\{^1H\}$ NMR (in $CDCl_3$): $\delta = 81.06$ ppm. Anal. Calcd C 36.82, H 5.18. Found C 36.47, H 5.25.

Preparation of $Ru_6(CO)_{17}(\mu_6\text{-}C)[Pd(PBu^t_3)]_2$, 11. A 20.0 mg amount of **9** (0.018 mmol) was dissolved in 25 mL of CH_2Cl_2. To this solution was added 29.3 mg of $Pd(PBu^t_3)_2$ (0.057 mmol), and the solution then was stirred at 25 °C for 30 min. The product was separated by TLC on silica gel by using 3:1 hexane/methylene chloride solvent mixture to yield 10.3 mg (33%) of $Ru_6(CO)_{17}(\mu_6\text{-}C)[Pd(PBu^t_3)]_2$, **11**. Spectral data for **11**: IR ν_{CO} (cm^{-1} in hexane): 2074 (w), 2046 (m), 2038 (vs), 2025 (m, sh), 2019 (s), 1880 (w, br), 1825 (w, br). ^1H NMR (in $CDCl_3$): $\delta = 1.46$ ppm (d, CH_3, $^3J_{P-H} = 12.6$ Hz). $^{31}P\{^1H\}$ NMR (in $CDCl_3$): $\delta = 82.28$ ppm. Anal. Calcd C 29.45, H 3.15. Found C 29.71, H 2.99.

Preparation of $Ru_6(CO)_{17}(\mu_6\text{-}C)[Pt(PBu^t_3)]$, 12, and $Ru_6(CO)_{17}(\mu_6\text{-}C)[Pt(PBu^t_3)]_2$, 13. A 17.7 mg amount of **9** (0.016 mmol) was dissolved in 15 mL of CH_2Cl_2 in a 25-mL three-neck round-bottom flask. To this was added 14.7 mg of $Pt(PBu^t_3)_2$ (0.032 mmol), and the reaction mixture was then stirred at room temperature for 30 min. The solvent was removed in vacuo, and the products were separated by TLC by using a 4:1 hexane/methylenechloride solvent mixture as the developing solvent to yield 3.2 mg (11%) of $Ru_6(CO)_{17}(\mu_6\text{-}C)[Pt(PBu^t_3)]$, **12**, and 5.8 mg (24%) of $Ru_6(CO)_{17}(\mu_6\text{-}C)[Pt(PBu^t_3)]_2$, **13**. Spectral data for **12**: IR ν_{CO} (cm^{-1} in CH_2Cl_2): 2085 (w), 2068 (w), 2049 (vs), 2037 (s). ^1H NMR (in $CDCl_3$): $\delta = 1.52$ ppm (d, 27H, CH_3, $^3J_{P-H} = 13$ Hz). $^{31}P\{^1H\}$ NMR (in $CDCl_3$): $\delta = 116.76$ ppm (s, 1P, $^1J_{Pt-P} = 6025$ Hz). Anal. Calcd C 24.14, H 1.81. Found C 24.06, H 1.70. Spectral data for **13**: IR ν_{CO} (cm^{-1} in CH_2Cl_2): 2074 (w), 2060 (w), 2035 (vs), 2014 (s), 1821 (w). ^1H NMR (in CD_2Cl_2): $\delta = 1.48$ ppm (d, 54H, CH_3, $^3J_{P-H} = 6.4$ Hz). $^{31}P\{^1H\}$ NMR (in CD_2Cl_2): $\delta = 117.37$ ppm (s, 1P, $^1J_{Pt-P} = 5870$ Hz). Anal. Calcd C 26.69, H 2.86. Found C 26.78, H 2.76.

Preparation of $Ru_6(CO)_{14}(\eta^6\text{-}C_6H_6)(\mu_6\text{-}C)[Pd(PBu^t_3)]$, 15. In 30 mL of $CHCl_2$ was dissolved 24.0 mg of **14** (0.022 mmol). To this solution over a 10-min period at room temperature was added 11.0 mg (0.022 mmol) of $Pd(PBu^t_3)_2$ dissolved in 8 mL of CH_2Cl_2. The solvent was then removed in vacuo, and the products were separated by TLC by using a 6:5 hexane/methylenechloride solvent mixture as the developing solvent. This yielded 7.5 mg of a brown band and 12.3 mg (51%) of the starting material, **15**. The $^{31}P\{^1H\}$ NMR spectrum of the brown band showed two resonances later assigned to the two products $Ru_6(CO)_{14}(\eta^6\text{-}C_6H_6)(\mu_6\text{-}C)[Pd(PBu^t_3)]$, **15**, and $Ru_6(CO)_{14}(\eta^6\text{-}C_6H_6)(\mu_6\text{-}C)[Pd(PBu^t_3)]_2$, **16**. From integration of these two resonances product **15** was obtained in 22% yield (6.6 mg), and product **16** was obtained in 2% yield (0.9 mg). NOTE: Both compounds **15** and **16** have the same R_f value and thus cannot be separated from each other by TLC. Analytically pure compound **15** was obtained by growing crystals by slow evaporation of solvent from a solution of the brown band from a hexane/methylene chloride solvent mixture

(14) Nicholls, J. N.; Vargas, M. D.; Hriljac, J.; Sailor, M. *Inorg. Synth.* **1989**, *26*, 283.
(15) Adams R. D.; Wu, W. *Polyhedron* **1992**, *11*, 2123.
(16) Otsuka, S.; Yoshida, T.; Matsumoto, M.; Nakatsu, K. *J. Am. Chem. Soc.* **1976**, *98*, 5850.

at 5 °C. Spectral data for **15**: IR ν_{CO} (cm^{-1} in CH_2Cl_2): 2064 (m), 2018 (s), 1990 (w, sh), 1971 (w, sh), 1815(vw, br). ^1H NMR (in $CDCl_3$): $\delta = 5.30$ ppm (s, 6H, C_6H_6), $\delta = 1.50$ ppm (d, 27H, CH_3, $^3J_{P-H} = 12$ Hz). $^{31}P\{^1H\}$ NMR (in $CDCl_3$): $\delta = 79.65$ ppm. Anal. Calcd C 28.36, H 2.36. Found C 28.70, H 2.58.

Preparation of $Ru_6(CO)_{14}(\eta^6\text{-}C_6H_6)(\mu_6\text{-}C)[Pd(PBu^t_3)]_2$, 16. A 19.0 mg (0.017 mmol) amount of **14** was dissolved in 40 mL of CH_2Cl_2. A 9 mg amount (0.018 mmol) of $Pd(PBu^t_3)_2$ was added, and the reaction mixture was stirred at room temperature for 15 min. At this time another equivalent of $Pd(PBu^t_3)_2$ (9 mg) was added to the reaction mixture and allowed to stir for a further 15 min. This addition procedure was repeated two more times at 15-min intervals. At the end of 1 h a total of 36 mg of $Pd(PBu^t_3)_2$ had been added. The solvent was then removed in vacuo, and the products were separated by TLC by using a 6:5 hexane/methylenechloride solvent mixture as the developing solvent to yield 13.0 mg of a brown band. A $^{31}P\{^1H\}$ NMR spectrum of the brown band showed that compound **15** was obtained in 10% yield (2.5 mg) and compound **16** in 35% yield (10.5 mg). Analytically pure **16** was obtained by growing crystals by slow evaporation of solvent from a hexane/methylene chloride solution of the brown band at 25 °C. Spectral data for **16**: IR ν_{CO} (cm^{-1} in CH_2Cl_2): 2054 (m), 2042 (w), 2002(s), 1972 (w, sh), 1810 (w, br). ^1H NMR (in $CDCl_3$): $\delta = 5.12$ ppm (s, 6H, C_6H_6), $\delta = 1.51$ ppm (d, 27H, CH_3, $^3J_{P-H} = 12$ Hz). $^{31}P\{^1H\}$ NMR (in $CDCl_3$): $\delta = 81.12$ ppm. Anal. Calcd C 31.65, H 3.52. Found C 31.72, H 3.65.

Crystallographic Analysis. Blue crystals of **10** were obtained by crystallization from a hexane/methylene chloride solution at −80 °C. Dark-red single crystals of **11**, **12**, **13**, and **15** suitable for diffraction analysis were grown by slow evaporation of solvent from solutions of the pure compound in hexane/methylene chloride solvent mixture at 5 °C. Dark-red single crystals of **16** were grown similarly by evaporation of solvent from a hexane/methylene chloride solvent mixture at 25 °C. Each data crystal was glued onto the end of a thin glass fiber. X-ray intensity data were measured using a Bruker SMART APEX CCD-based diffractometer using Mo Kα radiation ($\lambda = 0.71073$ Å). The raw data frames were integrated with the SAINT+ program using a narrow-frame integration algorithm.[17] Correction for the Lorentz and polarization effects were also applied by using the program SAINT. An empirical absorption correction based on the multiple measurement of equivalent reflections was applied by using the program SADABS. All structures were solved by a combination of direct methods and difference Fourier syntheses and were and refined by full-matrix least-squares on F^2, by using the SHELXTL software package.[18] All nonhydrogen atoms were refined with anisotropic thermal parameters. Hydrogen atoms were placed in geometrically idealized positions and included as standard riding atoms during least-squares refinements. Crystal data, data collection parameters, and results of the analyses for compounds **10** and **11** are listed in Table 1, for compounds **12** and **13** in Table 2, and for compounds **15** and **16** in Table 3.

Compounds **10**, **13**, and **16** crystallized in the monoclinic crystal system. The space groups $P2_1/c$ (for compounds **10** and **13**) and $P2_1/n$ (for compound **16**) were identified uniquely on the basis of the systematic absences observed during the collection of the intensity data. For compound **13** there are two independent formula equivalents of the complex present in the asymmetric unit. Compounds **11** and **12** crystallized in the

Table 1. Crystallographic Data for Compounds **10** and **11**

	10	**11**
empirical formula	$Pd_3Ru_3P_3O_{12}C_{48}H_{81}$	$Pd_2Ru_6P_2O_{17}C_{42}H_{54}$
formula weight	1565.45	1712.01
crystal system	monoclinic	orthorhombic
lattice parameters		
a (Å)	24.663(2)	15.1983 (11)
b (Å)	14.9128 (13)	19.7491 (15)
c (Å)	16.4277 (14)	35.841 (3)
α (deg)	90	90
β (deg)	91.909 (2)	90
γ (deg)	90	90
V (Å^3)	6038.6 (9)	10757.8 (14)
space group	$P2_1/c$	$P2_12_12_1$
Z value	4	8
ρ_{calc} (g/cm^3)	1.722	2.114
μ (Mo Kα) (mm^{-1})	1.737	2.413
T (K)	190	190
$2\Theta_{max}$ (°)	46.62	52.8
no. obs. ($I > 2\sigma(I)$)	4571	20374
no. parameters	648	1279
goodness of fit	0.986	0.951
max shift in cycle	0.000	0.003
residuals: R1; wR2[a]	0.0437; 0.0759	0.0296; 0.0559
absorption correction, max/min	none	SADABS 0.74; 0.48
largest peak in final diff. map (e$^-$/Å^3)	0.705	0.791

[a] $R = \Sigma_{hkl}(||F_{obs}| - |F_{calc}||)/\Sigma_{hkl}|F_{obs}|$; $R_w = [\Sigma_{hkl}w(|F_{obs}| - |F_{calc}|)^2/\Sigma_{hkl}wF_{obs}^2]^{1/2}$, $w = 1/\sigma^2(F_{obs})$; GOF $= [\Sigma_{hkl}w(|F_{obs}| - |F_{calc}|)^2/(n_{data} - n_{vari})]^{1/2}$.

Table 2. Crystallographic Data for Compounds **12** and **13**

	12	**13**
empirical formula	$PtRu_6PO_{17}C_{30}H_{27}$	$Pt_2Ru_6P_2O_{17}C_{42}H_{54}$
formula weight	1492.00	1889.39
crystal system	orthorhombic	monoclinic
lattice parameters		
a (Å)	12.2489 (5)	18.1870 (5)
b (Å)	19.8587 (8)	19.6886 (6)
c (Å)	16.4570 (6)	31.1190 (9)
α (deg)	90	90
β (deg)	90	95.0310 (10)
γ (deg)	90	90
V (Å^3)	4003.1 (3)	11100.1 (6)
space group	$Pna2_1$	$P2_1/c$
Z value	4	8
ρ_{calc} (g/cm^3)	2.476	2.261
μ (Mo Kα) (mm^{-1})	5.792	6.726
T (K)	293	293
$2\Theta_{max}$ (°)	52.5	50.1
no. obs. ($I > 2\sigma(I)$)	7207	13429
no. parameters	506	1279
goodness of fit	1.035	0.964
max shift in cycle	0.002	0.002
residuals: R1; wR2[a]	0.0351; 0.0590	0.0435; 0.0669
absorption correction, max/min	SADABS 1.00; 0.86	SADABS 1.00; 0.76
largest peak in final diff. map (e$^-$/Å^3)	0.703	1.085

[a] $R = \Sigma_{hkl}(||F_{obs}| - |F_{calc}||)/\Sigma_{hkl}|F_{obs}|$; $R_w = [\Sigma_{hkl}w(|F_{obs}| - |F_{calc}|)^2/\Sigma_{hkl}wF_{obs}^2]^{1/2}$, $w = 1/\sigma^2(F_{obs})$; GOF $= [\Sigma_{hkl}w(|F_{obs}| - |F_{calc}|)^2/(n_{data} - n_{vari})]^{1/2}$.

(17) SAINT+, version 6.02a; Bruker Analytical X-ray System, Inc., Madison, Wisconsin, 1998.
(18) Sheldrick, G. M. SHELXTL, version 5.1; Bruker Analytical X-ray Systems, Inc., Madison, Wisconsin, 1997.

Table 3. Crystallographic Data for Compounds **15** and **16**

	15	**16**
empirical formula	$PdRu_6PO_{14}C_{33}H_{33}$	$Pd_2Ru_6P_2O_{14}C_{45}H_{60}$
formula weight	1397.38	1706.09
crystal system	triclinic	monoclinic
lattice parameters		
a (Å)	8.9793 (9)	15.2586 (6)
b (Å)	13.7655 (14)	16.2472 (6)
c (Å)	17.1762 (18)	22.7817 (9)
α (deg)	77.464(2)	90
β (deg)	88.967(2)	102.8920 (10)
γ (deg)	81.998(2)	90
V (Å^3)	2052.1 (4)	5505.4 (4)
space group	$P\bar{1}$	$P2_1/n$
Z value	2	4
ρ_{calc} (g/cm^3)	2.261	2.058
μ (Mo Kα) (mm^{-1})	2.677	2.353
T (K)	293	293
$2\Theta_{max}$ (deg)	52.0	52.0
no. obs. ($I > 2\sigma(I)$)	6010	7747
no. parameters	505	640
goodness of fit	1.060	1.002
max shift in cycle	0.002	0.002
residuals: R1; wR2[a]	0.0496; 0.1061	0.0462; 0.0937
absorption correction,	SADABS	SADABS
max/min	1.00; 0.81	1.00; 0.85
largest peak in	0.957	0.832
final diff. map (e$^-$/Å^3)		

[a] $R = \Sigma_{hkl}(||F_{obs}| - |F_{calc}||)/\Sigma_{hkl}|F_{obs}|$; $R_w = [\Sigma_{hkl}w(|F_{obs}| - |F_{calc}|)^2/\Sigma_{hkl}wF_{obs}^2]^{1/2}$, $w = 1/\sigma^2(F_{obs})$; GOF $= [\Sigma_{hkl}w(|F_{obs}| - |F_{calc}|)^2/(n_{data} - n_{vari})]^{1/2}$.

orthorhombic crystal system. The space group $P2_12_12_1$ was identified uniquely on the basis of the systematic absences observed during the collection of the intensity data for compounds **11**. For compound **12** the space groups $Pna2_1$ and *Pnma* were indicated by the systematic absences in the data. The former space group was assumed and confirmed by the solution and refinement of the structure. For compound **11** there are two independent formula equivalents of the complex present in the asymmetric unit. Compound **15** crystallized in the triclinic crystal system. The space group $P\bar{1}$ was assumed and confirmed by the successful solution and refinement of the structure.

Molecular Orbital Calculations. All molecular orbital calculations reported here are from the Fenske−Hall method.[19] Fenske−Hall calculations were performed utilizing a graphical user interface developed[20] to build inputs and view outputs from stand-alone Fenkse−Hall (version 5.2) and MOPLOT2[21] binary executables. Contracted double-ζ basis sets were used for the Ru and Pd 4d, P 3p, and C and O 2p atomic orbitals. The Fenske−Hall scheme is a nonempirical, approximate method that is capable of calculating molecular orbitals for very large transition metal systems and has built-in fragment analysis routines that allow one to assemble transition metal cluster structures from the corresponding ligated fragments.

Results and Discussion

Because of the great steric bulk of tri-*tert*-butylphosphine, the compounds $M(PBu^t_3)_2$, M = Pd and Pt, are air stable even

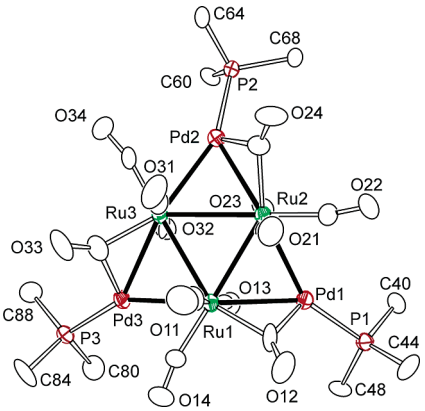

Figure 1. ORTEP diagram of $Ru_3(CO)_{12}[Pd(PBu^t_3)]_3$, **10**, showing thermal ellipsoids at 50% probability. The methyl groups have been omitted for clarity.

Table 4. Selected Intramolecular Distances and Angles for $Ru_3(CO)_{12}[Pd(PBu^t_3)]_3$, **10**[a]

(a) Distances

atom	atom	distance (Å)	atom	atom	distance (Å)
Ru(1)	Pd(1)	2.7877(12)	Ru(3)	Pd(2)	2.8310(12)
Ru(1)	Pd(3)	2.7962(12)	Ru(3)	Pd(3)	2.8050(12)
Ru(1)	Ru(2)	2.9191(12)	Pd(1)	P(1)	2.365(3)
Ru(1)	Ru(3)	2.9418(12)	Pd(2)	P(2)	2.366(3)
Ru(2)	Pd(1)	2.8398(11)	Pd(3)	P(3)	2.369(3)
Ru(2)	Pd(2)	2.7928(12)	O(av)	C(av)	1.166(12)
Ru(2)	Ru(3)	2.9690(12)			

(b) Angles

atom	atom	atom	angle (deg)	atom	atom	atom	angle (deg)
Pd(1)	Ru(1)	Pd(3)	144.56(4)	Pd(3)	Ru(1)	Ru(2)	117.22(4)
Pd(1)	Ru(1)	Ru(2)	59.63(3)	Pd(3)	Ru(1)	Ru(3)	58.46(3)
Pd(1)	Ru(1)	Ru(3)	116.18(4)	Ru(2)	Ru(1)	Ru(3)	60.87(3)

though they have only two phosphine ligands. The reaction of $Ru_3(CO)_{12}$ with an excess of $Pd(PBu^t_3)_2$ at room temperature afforded the tripalladium complex $Ru_3(CO)_{12}[Pd(PBu^t_3)]_3$, **10**, in 49% yield, eq 1.

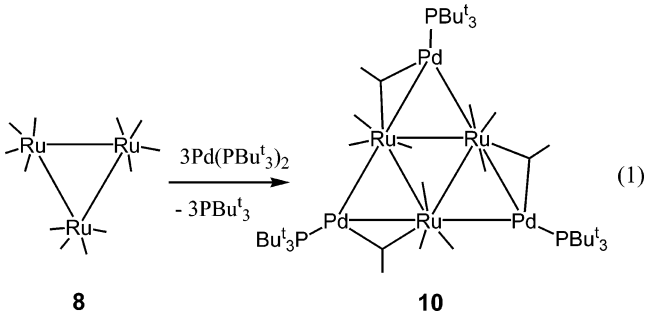

(1)

Compound **10** was characterized by a combination of IR, ^{1}H- and ^{31}P NMR, and single-crystal X-ray diffraction analyses. An ORTEP diagram of the molecular structure of **10** is shown in Figure 1. Selected bond distances and angles are listed in Table 4. The compound has a "raft-like" structure with a triangular Ru_3 unit in the center. Each edge of the Ru_3 group is bridged by a $Pd(PBu^t_3)$ group. The six-metal cluster is not planar, and each Pd atom is displaced by 0.6964(16)−0.9866(15) Å out of the Ru_3 plane to the same side. Each ruthenium atom contains three linear terminal CO ligands plus one CO ligand that forms a bridge to a palladium atom. Because there was no loss of a

(19) Hall, M. B.; Fenske, R. F. *Inorg. Chem.* **1972**, *11*, 768−775.
(20) Manson, J.; Webster, C. E.; Hall, M. B. JIMP Development Version 0.1 (built for Windows PC and Redhat Linux); Department of Chemistry, Texas A&M University, College Station, TX 77842 (http://www.chem.tamu.edu/jimp/).
(21) MOPLOT2: for orbital and density plots from linear combinations of Slater or Gaussian type orbitals, version 2.0, June 1993; Dennis L. Lichtenberger, Department of Chemistry, University of Arizona, Tucson, AZ 85721.

Scheme 1

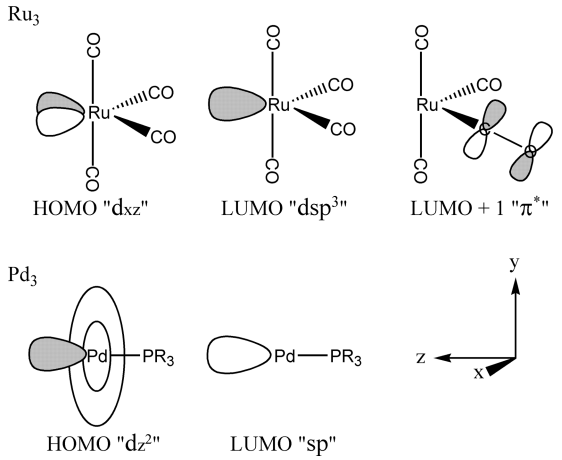

CO ligand from **8**, compound **10** can be viewed most simply as a tris-Pd(PBu^t_3) adduct of it with the Pd(PBu^t_3) groups being generated from Pd(PBu^t_3)$_2$ by the loss of one of its PBu^t_3 ligands. The Ru−Ru bonds, Ru(1)−Ru(2) = 2.9191(12) Å, Ru(1)−Ru(3) = 2.9418(12) Å, Ru(2)−Ru(3) = 2.9690(12) Å, are slightly longer than those in $Ru_3(CO)_{12}$, 2.854(1) Å,[22a] but are similar to the hydride-bridged Ru−Ru bond distances found in $H_2Ru_4(CO)_{13}$, 2.936(1)−2.955(1) Å.[22b]

A simple model for the bonding of the palladium atoms to the Ru−Ru bonds can be constructed as follows: the Pd(PBu^t_3) fragment contains only 12 valence electrons and will be a strong Lewis acid. If two electrons from a Ru−Ru bond are shared with the proximate Pd atom, then a 3-center/2-electron $PdRu_2$ bond would be formed, and the electron count at the palladium atom would be increased formally to 14, as it was in the parent Pd(PBu^t_3)$_2$ (see model A).

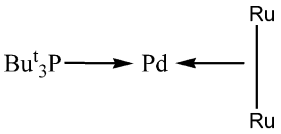

A

This is conceptually similar to the well-known protonation of the metal−metal bonds of polynuclear metal complexes that occurs in strong protic media.[23]

The Pd−Ru interactions in **10** are, however, more complex than this simple model and include additional stablization by bonding to a bridging carbonyl ligand which was included in the refined Fenske−Hall molecular orbital model described as follows. The entire molecule can be viewed as an assembly of three $Ru(CO)_4$ units and three Pd(PR_3) units, but it is not obvious why the dimer of trimers is distorted to a C_3-like structure rather than having a higher symmetry D_3-like structure. The bridging CO was assigned to Ru because its σ-donor orbital was directed more toward Ru than Pd. The key low-lying orbitals are shown diagrammatically in Scheme 1. The $Ru(CO)_4$ appears most like a trigonal bipyramid with a missing ligand. As this neutral fragment would have a d^8 configuration, the highest-occupied molecular orbital (HOMO) is the d_{xz}, the d orbital that would have been stabilized by the missing CO in the fully ligated $Ru(CO)_5$ molecule (see Scheme 1). The lowest-unoccupied molecular orbital (LUMO) is the "dsp^3" hybrid that would have been destabilized by accepting the fifth CO's lone pair (see Scheme 1). The last orbital of importance on the $Ru(CO)_4$ fragment is the low-lying π^* orbital on the distorted CO (LUMO+1). This distortion (a Ru−C−O angle of ∼140° rather than 180°) arises from the clockwise (or counterclockwise) twisting of each $Ru(CO)_4$ unit to place one CO closer to each Pd. The distortion lowers the energy of this LUMO+1 orbital because it is now less effective in back-bonding to the Ru. We will return to the origin of this twisting and subsequent distortion later after describing the bonding in the structure as found. The key orbitals of the Pd(PR_3) fragment are somewhat simpler (see Scheme 1). The HOMO is the z^2, the d orbital pointing away from the only ligand in this d^{10} fragment, while the LUMO is the "sp" hybrid pointing in the same direction.

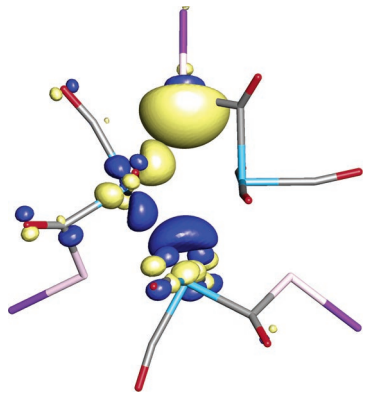

Figure 2. Fragment molecular orbitals that produce the 3-center/2-electron bonds (one of three by symmetry), which constitute the principal metal-to-metal bonding interactions of $Ru_3(CO)_{12}[Pd(PBu^t_3)]_3$.

When three $Ru(CO)_4$ and three Pd(PR_3) fragments assemble into the cluster, the principal metal−metal bonding arises from the HOMO of one Ru donating electron density into both the LUMO on the Pd opposite the bridging CO and the LUMO of the Ru on the first Ru's other side. Three of these 3-center/2-electron bonds constitute the principal metal-to-metal bonding molecular orbitals; one of these interactions is shown in Figure 2, which shows the actual fragment MOs from the Fenske−Hall calculation. Here, the same fragment orbitals as shown diagrammatically in Scheme 1 are shown in their correct relationship to each other. An important secondary interaction is shown in Figure 3, where the HOMO of the Pd(PR_3) fragment (in particular the "donut" of the d_{z^2}) donates electron density to the LUMO+1 of the $Ru(CO)_4$, the π^* orbital of the semibridging CO.

Now, one may wonder why the $Ru(CO)_4$ distorts such that the secondary interaction described above is unsymmetrical. In a more symmetrical structure the CO's on both sides of the Ru could accept electron density from the Pd HOMO. Therefore, the distortion most likely has another origin, i.e., the bent Ru−C−O structure and the subsequent "one-side" Pd to CO(Ru) back-bonding is a response to the distortion and not the driving force.

(22) (a) Churchill, M. R.; Hollander, F. J.; Hutchinson, J. P. *Inorg. Chem.* **1977**, *16*, 2655. (b) Rheingold, A. L.; Haggerty, B. S.; Geoffroy, G. L.; Han, S.-H. *J. Organomet. Chem.* **1990**, *384*, 209.

(23) (a) Nataro, C.; Thomas, L. M.; Angelici, R. J. *Inorg. Chem.* **1997**, *36*, 6000. (b) Kristjansdottir, S. S.; Moody, A. E.; Weberg, R. T.; Norton, J. R. *Organometallics* **1988**, *7*, 1983. (c) Wlaker, H. W.; Pearson, R. G.; Ford, P. C. *J. Am. Chem. Soc.* **1983**, *105*, 1179. (d) Deeming, A. J.; Johnson, B. F. G.; Lewis, J. *J. Chem. Soc. (A)* **1970**, 2967. (e) Knight, J.; Mays, M. J *J. Chem. Soc. (A)* **1970**, 711.

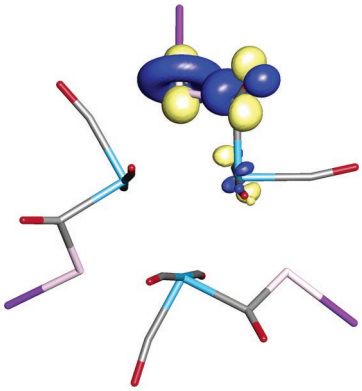

Figure 3. Pd(PR_3) fragment HOMO that donates electron density to the LUMO+1 of the Ru$(CO)_4$ fragment, primarily a π^* orbital of the semibridging CO.

Scheme 2

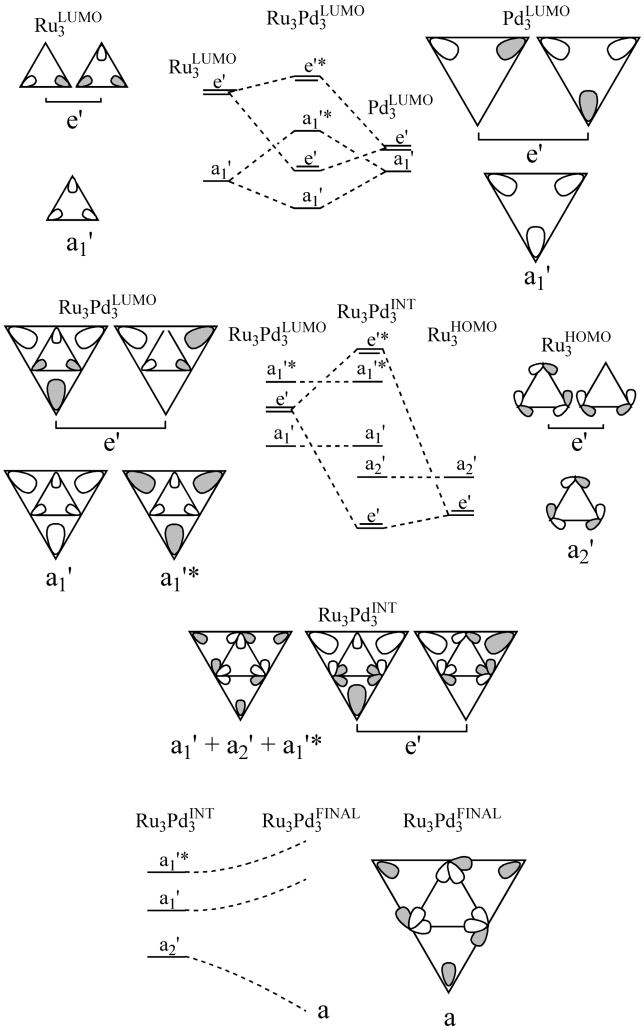

The driving force for the distortion arises from a second-order Jahn−Teller(JT) effect,[24] because in a high-symmetry point group, such as D_{3h} or C_{3v}, the irreducible representations of symmetry-adapted linear combinations of the Ru$(CO)_4$ HOMOs have an incomplete correspondence to irreducible representations of the symmetry adapted LUMOs of the neighboring fragments. Thus, the Ru$(CO)_4$ twists to reduce the symmetry and maximize its interaction with its neighbors. A complete analysis of the second-order JT effect is illustrated in Scheme 2. For the purpose of this analysis, the molecular electronic structure will be represented simply by two triangular metal clusters, one with three Ru fragments and one larger triangle, rotated 60°, with three Pd fragments. For the main metal-to-metal bonding there are three donor orbitals on the Ru (Ru^{HOMO}) and six acceptor orbitals, three on Ru (Ru^{LUMO}) and three on Pd (Pd^{LUMO}). In the highest possible local symmetry, D_{3h}, the Ru_3^{LUMO} and Pd_3^{LUMO} orbitals transform as $\mathbf{a_1}'$ and $\mathbf{e}'$, as shown at the top of Scheme 2. These two sets of LUMOs interact with each other (as shown by the orbital interaction diagram at the top of Scheme 2) to form in-phase, lower-lying combinations and out-of-phase higher-lying combinations. Thus, one now has a set of strong acceptor orbitals involving all six metal atoms that transform as $\mathbf{a_1}'$, $\mathbf{e}'$, and $\mathbf{a_1}'^*$ (the $Ru_3Pd_3^{LUMO}$ orbitals shown in Scheme 2). The primary metal-to-metal bonding occurs when these $Ru_3Pd_3^{LUMO}$ orbitals accept electron density from the Ru_3^{HOMO} orbitals. The symmetry-adapted linear combinations of the latter orbitals are shown interacting with the $Ru_3Pd_3^{LUMO}$ set in the center of Scheme 2. However, since the Ru_3^{HOMO} set transforms as $\mathbf{a_2}'$ and $\mathbf{e}'$, not $\mathbf{a_1}'$ and $\mathbf{e}'$, there is a symmetry mismatch in D_{3h} or C_{3v} ($\mathbf{a_2}$, $\mathbf{a_1}$, and $\mathbf{e}$) point groups. Thus, all three pairs of electrons from the Ru_3^{HOMO} set cannot be used for bonding in a high-symmetry situation. This dilemma is illustrated in the second orbital interaction diagram in Scheme 2, which shows a suitable bonding $Ru_3Pd_3^{INT}$ interaction for the $\mathbf{e}'$ arising from the $\mathbf{e}'$ of the Ru_3^{HOMO} donating to the $\mathbf{e}'$ of the $Ru_3Pd_3^{LUMO}$. However, in this high-symmetry both the occupied Ru_3^{HOMO} $\mathbf{a_2}'$ and the unoccupied $Ru_3Pd_3^{LUMO}$ $\mathbf{a_1}'$ and $\mathbf{a_1}'^*$ must remain nonbonding as the energy diagram shows and as is illustrated in the linear combination $\mathbf{a_1}' + \mathbf{a_2}' + \mathbf{a_1}'^*$, where one can see that the $\mathbf{a_2}'$ combination has zero overlap by symmetry with $\mathbf{a_1}'$ and $\mathbf{a_1}'^*$. The dilemma can be resolved by twisting the Ru$(CO)_4$ so that the symmetry drops to the C_3 point group and the $\mathbf{a_1}'$ and $\mathbf{a_2}'$ both become $\mathbf{a}$ in $Ru_3Pd_3^{FINAL}$ and their mutual interaction will stabilize the occupied combination as shown at the bottom of Scheme 2; the HOMO for $Ru_3Pd_3^{FINAL}$ is shown in Figure 4.

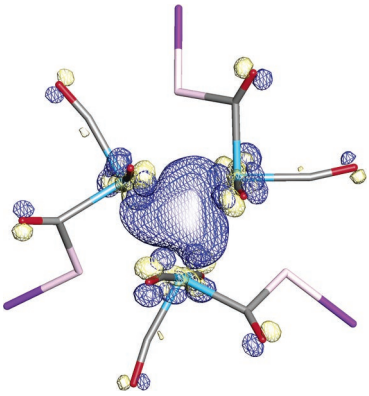

Figure 4. HOMO of the $Ru_3(CO)_{12}[Pd(PBu^t_3)]_3$ cluster.

An analysis of the overlap populations both among the fragments and between individual metal atoms suggests that there are direct Ru−Ru bonds and direct Ru−Pd bonds along

(24) *The Jahn−Teller Effect and Vibronic Interactions in Modern Chemistry*; Bersuker, I. B., Ed.; Plenum Press: New York, 1984. *Orbital Interactions in Chemistry*; Albright, T. A., Berdett, J. K., Whangbo, M. W., Eds.; John Wiley and Sons: New York, 1985; pp 95−100; *Symmetry Rules for Chemical Reactions: Orbital Topology and Elementary Processes*; Pearson, R. G., Ed.; John Wiley and Sons: New York, 1976; pp 75−82.

Scheme 3

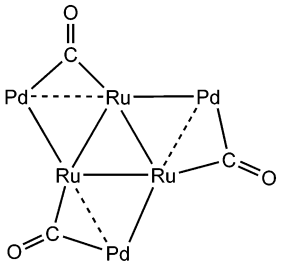

Table 5. Selected Intramolecular Distances and Angles for $Ru_6(CO)_{17}(\mu_6\text{-}C)[Pd(PBu^t_3)]_2$, **11**[a]

(a) Distances

atom	atom	distance (Å)	atom	atom	distance (Å)
Pd(1)	P(1)	2.4276(14)	Ru(1)	Ru(5)	2.8656(6)
Pd(1)	Ru(2)	2.7790(6)	Ru(2)	Ru(3)	2.9749(6)
Pd(1)	Ru(3)	2.8319(6)	Ru(2)	Ru(5)	2.8590(6)
Pd(2)	P(2)	2.4350(13)	Ru(2)	Ru(6)	2.8619(6)
Pd(2)	Ru(5)	2.8453(6)	Ru(3)	Ru(4)	2.8643(6)
Pd(2)	Ru(6)	2.8011(6)	Ru(3)	Ru(6)	2.8584(6)
Pd(3)	P(3)	2.4343(14)	Ru(4)	Ru(5)	2.9588(6)
Pd(3)	Ru(7)	2.7806(6)	Ru(4)	Ru(6)	2.9363(6)
Pd(3)	Ru(9)	2.8423(6)	Ru(5)	Ru(6)	2.9936(6)
Pd(4)	P(4)	2.3943(14)	Ru(1)	C(1)	2.067(5)
Pd(4)	Ru(10)	2.8050(6)	Ru(2)	C(1)	2.046(5)
Pd(4)	Ru(11)	3.0531(6)	Ru(3)	C(1)	2.063(5)
Pd(4)	Ru(12)	2.8828(6)	Ru(4)	C(1)	2.069(5)
Ru(1)	Ru(2)	3.0066(6)	Ru(5)	C(1)	2.065(5)
Ru(1)	Ru(3)	2.9482(6)	Ru(6)	C(1)	2.056(5)
Ru(1)	Ru(4)	2.8429(6)	O(av)	C(av)	1.15(1)

(b) Angles

atom	atom	atom	angle (deg)	atom	atom	atom	angle (deg)
Ru(2)	Pd(1)	Ru(3)	64.030(15)	Ru(11)	Pd(4)	Ru(12)	59.287(15)
Ru(5)	Pd(2)	Ru(6)	64.029(15)	Ru(1)	Ru(2)	Ru(6)	89.198(16)
Ru(7)	Pd(3)	Ru(9)	64.431(15)	Ru(1)	Ru(3)	Ru(6)	90.431(17)
Ru(10)	Pd(4)	Ru(12)	65.830(16)	Ru(1)	C(1)	Ru(6)	177.4(3)
Ru(10)	Pd(4)	Ru(11)	59.756(15)	Ru(3)	C(1)	Ru(5)	178.7(3)

[a] Estimated standard deviations in the least significant figure are given in parentheses.

the unbridged edges. However, along the CO-bridged Ru−Pd edge, there is significantly less direct Ru−Pd bonding,[25] but strong Ru−C(O)−Pd bonding. Thus, the single-best valence representation, which is constructed from both the orbital and overlap population analysis, is shown in Scheme 3.

The dipalladium complex $Ru_6(CO)_{17}(\mu_6\text{-}C)[Pd(PBu^t_3)]_2$, **11**, was formed in 33% yield from the reaction of $Ru_6(CO)_{17}(\mu_6\text{-}C)$, **9**, with $Pd(PBu^t_3)_2$ at room temperature. Compound **11** was characterized by a combination of IR, ^{1}H- and ^{31}P NMR, and single-crystal X-ray diffraction analyses. Selected bond distances and angles are listed in Table 5. The structure of **11** consists of an octahedral cluster of six ruthenium metal atoms with a carbon atom in the center, and two $Pd(PBu^t_3)$ groups coordinated to it. In the solid-state compound **11** exists as two isomers, and both isomers can be viewed as bis-$Pd(PBu^t_3)$ adducts of $Ru_6(CO)_{17}(\mu_6\text{-}C)$ as there was no loss of CO from the Ru_6 starting material. In one isomer the $Pd(PBu^t_3)$ groups bridge two edges, Ru(2)−Ru(3) and Ru(5)−Ru(6), of the Ru_6 octahedron, see Figure 5. In the other isomer, Figure 6, one $Pd(PBu^t_3)$ group bridges the Ru(7)−Ru(9) edge of the Ru_6 octahedron, while the other Pd-

(25) Bridging carbonyls can reduce direct M−M bonding character. Summerville, R. H.; Hoffmann, R. *J. Am. Chem. Soc.* **1979**, *101*, 3921. Macchi, P.; Sironi, A. *Coord. Chem. Rev.* **2003**, *238*, 383.

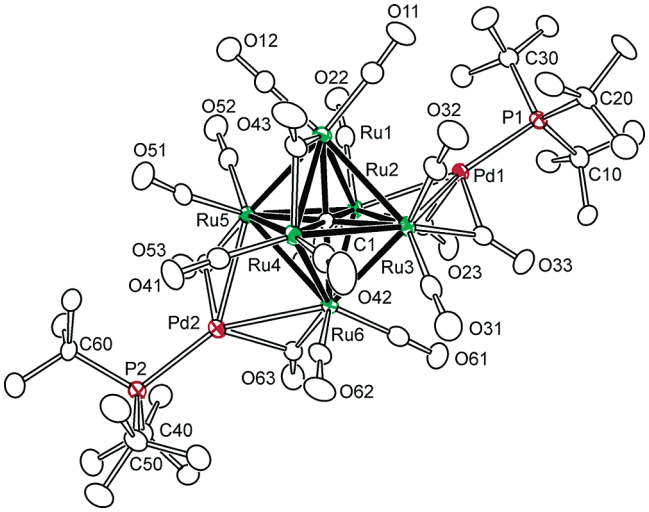

Figure 5. ORTEP diagram of the molecular structure of $Ru_6(CO)_{17}(\mu_6\text{-}C)[Pd(PBu^t_3)]_2$, **11**, showing thermal ellipsoids at 40% probability.

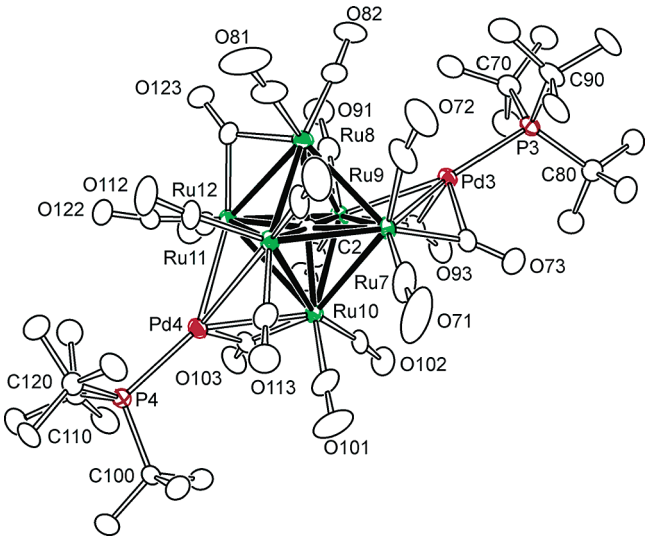

Figure 6. ORTEP diagram of the molecular structure of $Ru_6(CO)_{17}(\mu_6\text{-}C)[Pd(PBu^t_3)]_2$, **11**, isomer 2 showing thermal ellipsoids at 40% probability.

Scheme 4

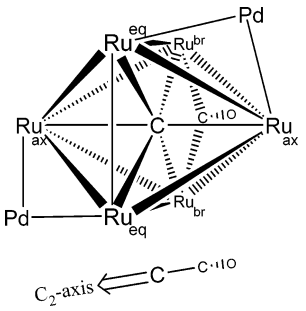

(PBu^t_3) group serves as a triple bridge capping the Ru(10)−Ru(11)−Ru(12) triangle with the Pd(4)−Ru(11) bond distance of 3.0531 Å being the longest. The Ru−Ru bond distances in the Ru_6 cluster are similar to those found in the parent compound.[26] Carbonyl ligands bridge from the Ru_6 cluster to the palladium atoms in both isomers.

(26) Braga, D.; Grepioni, F.; Dyson, P. J.; Johnson, B. F. G.; Frediani, P.; Bianchi, M.; Piacenti, F. *J. Chem. Soc., Dalton Trans.* **1992**, 2565.

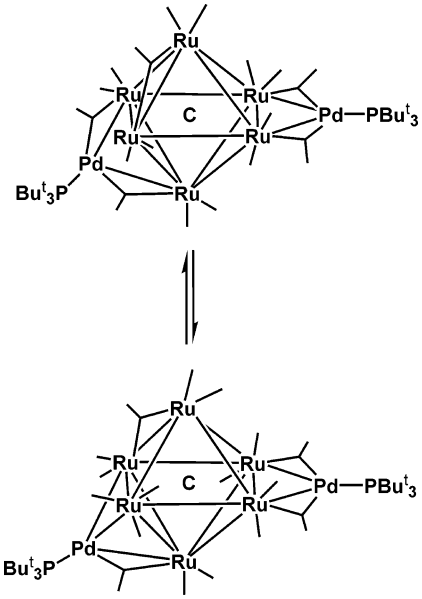

11

Molecular orbital calculations have also been performed for compound **11** and are described as follows. One can envision this $Ru_6C(CO)_{17}[Pd(PR_3)]_2$ cluster (see Scheme 4) being assembled from one central C atom, two sets of two $Ru(CO)_3$ fragments (forming axial (Ru_{ax}) and equatorial (Ru_{eq}) [$Ru(CO)_3]_2$ units), two $Ru(CO)_2$ fragments (Ru_{br}) bridged by one "extra" CO (forming a (μ-CO)[$Ru_{br}(CO)_2]_2$ unit), and two $Pd(PR_3)$ fragments. (In the text, orbitals from Ru_{ax}, Ru_{eq}, and Ru_{br} fragments will be designated with an appropriate suffix, e.g., **1a**-eq for the **1a** orbital of [$Ru_{eq}(CO)_3]_2$.) The key low-lying orbitals for $Ru(CO)_3$, $Ru(CO)_2$, $Pd(PR_3)$ units are illustrated in Schemes 1 and 5. In the neutral, d^8 $Ru(CO)_3$ fragment (Schemes 5 and 6), the d orbitals from two sets that reflect the character of their octahedral parentage: (1) three occupied orbitals (**1a$_1$** and **1e**) are stabilized by the carbonyl π^* like the parent octahedral t_{2g} set and (2) the **2e** orbitals with 2 e− are

Scheme 6

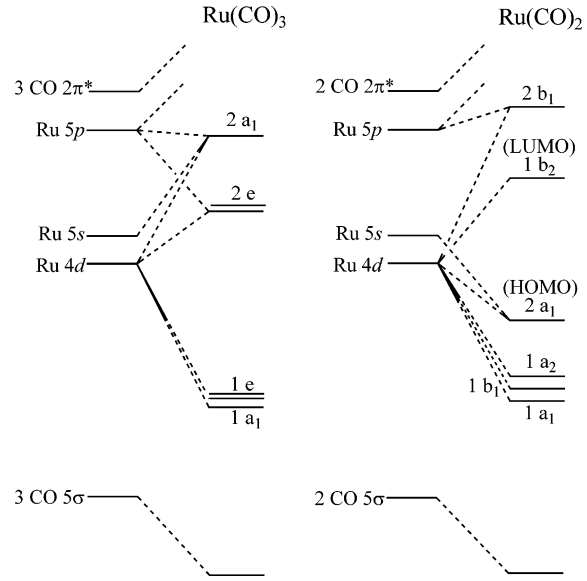

destabilized by the carbonyl σ like the parent octahedral e_g set. Removing one CO from the $Ru(CO)_3$ fragment generates the d^8 $Ru(CO)_2$ fragment, (Schemes 5 and 6) whose five orbitals with t_{2g} and e_g parentage are three low-lying orbitals (**1a$_1$**: mostly d_{z^2}; **1b$_1$**:d_{xz}; **1a$_2$**:d_{xy}), the HOMO (**2a$_1$**, mostly $d_{x^2-y^2}$), and the LUMO (**1b$_2$**:d_{yz}). The **2e** set for $Ru(CO)_3$ and the **1b$_2$** set for $Ru(CO)_2$ have some p character, which is not shown in the orbital representations of Scheme 5. The correspondence of the orbital fragments is as follows: **1a$_1$**, **1e**$_{d_{x^2-y^2}}$, **1e**$_{d_{xy}}$, **2e**$_{d_{xz}}$, and **2e**$_{d_{yz}}$ for $Ru(CO)_3$ correspond to **1b$_1$**, **1a$_1$**, **1a$_2$**, **2a$_1$**, and **1b$_2$** of $Ru(CO)_2$, respectively. The key orbital of the d^{10} $Pd(PR_3)$ fragment is the previously mentioned LUMO, the "sp" hybrid (see Scheme 1).

One may build up the complex by combining fragments sequentially. Using the extra CO to bridge the two $Ru(CO)_2$ units affords a (μ-CO)[$Ru_{br}(CO)_2]_2$ fragment (see Scheme 7). This combination of fragments produces eight key orbitals, **2a**-br, **1b**-br, **2b**-br, **3b**-br, **4a**-br, **5a**-br, **5b**-br, and **6a**-br (see

Scheme 5

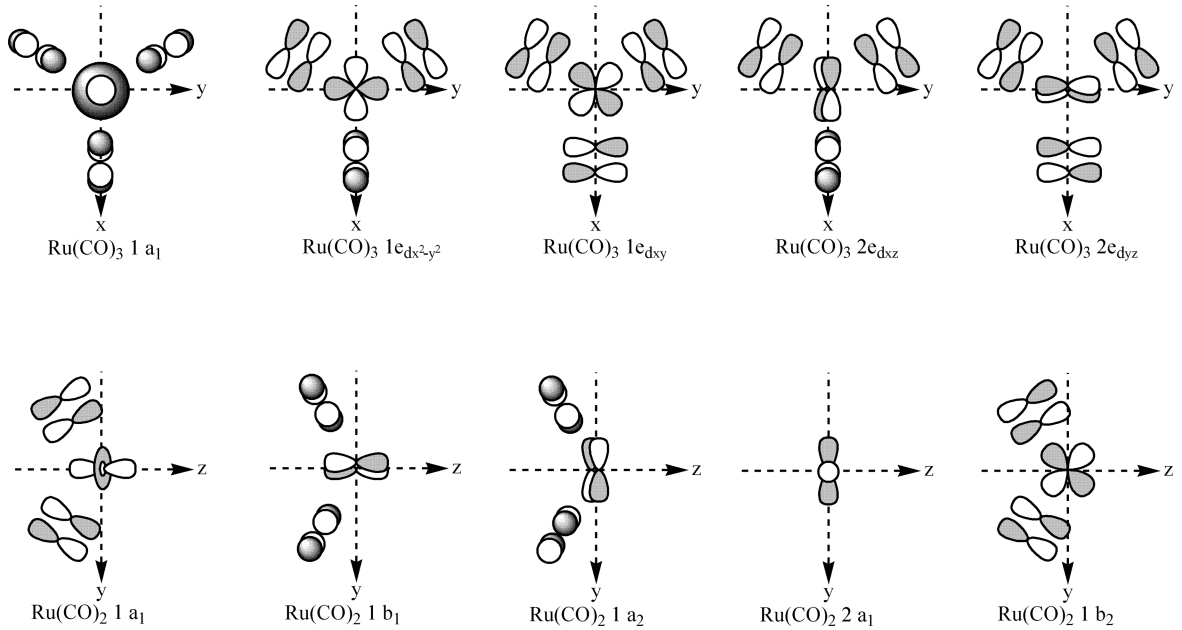

Scheme 7

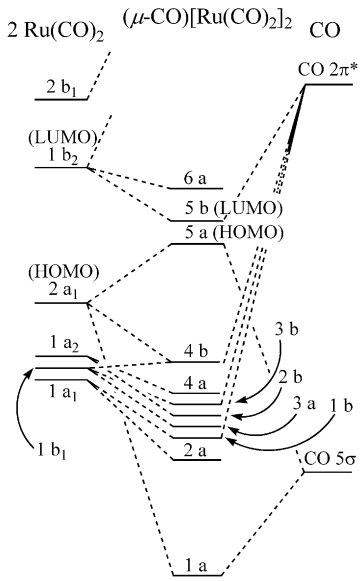

Scheme 8; note that idealized, higher-symmetry fragments are used for the orbital representations of (μ-CO)[$Ru_{br}(CO)_2]_2$, and contributions from the bridging CO, which is along the *z*-axis, are not shown). The $Ru(CO)_3$ fragments can be assembled as two sets of two. The two $Ru(CO)_3$ fragments that are opposite the two Ru_{br} of the (μ-CO)[$Ru_{br}(CO)_2]_2$ fragment combine to produce the equatorial fragment, $[Ru_{eq}(CO)_3]_2$, and the two remaining $Ru(CO)_3$ fragments combine to produce the axial fragment, $[Ru_{ax}(CO)_3]_2$. The molecular orbital diagrams for these two bis $Ru(CO)_3$ fragments are represented in Scheme 9, and the important orbitals from each one are represented in Schemes 10 and 11 (again, idealized, higher-symmetry fragments are used for the orbital representations of $[Ru_{eq}(CO)_3]_2$ and $[Ru_{ax}(CO)_3]_2$).

These two sets of $[Ru(CO)_3]_2$ fragments, the (μ-CO)[Ru_{br}-$(CO)_2]_2$ unit, and one C atom combine to form the core Ru_6C-$(CO)_{17}$ unit, which has seven orbitals important to cluster bonding in accord with electron-counting rules[27] (see Scheme 12 and Figure 7): one 7-center/2-electron (7c/2e−) bond containing central C s-character (**1a**) bonding to all Ru, one 5c/2e− bond (with four Ru) and two 7c/2e− bonds (with all Ru) containing central C p-character (**1b**, **2a**, and **2b**), two 6c/2e− bonds (**3a** and **3b** with all Ru), and one 2c/2e− bond (**4a** with the two Ru_{eq}). The **1a** orbital of $Ru_6C(CO)_{17}$ is formed by a combination of **1a**-br from (μ-CO)[$Ru_{br}(CO)_2]_2$, **1a**-eq and **2a**-eq (**2a**-eq is not pictured) from $[Ru_{eq}(CO)_3]_2$, and **1a**-ax and **2a**-ax (not pictured) from $[Ru_{ax}(CO)_3]_2$ with the central C s orbital. The **1b** orbital is formed by a combination of **1b**-br, **2b**-br, **1b**-eq, **2b**-eq, and **2b**-ax with the central C p_x and p_y orbitals. The **2a** orbital is formed by a combination of **1a**-eq, **1a**-ax, and **3a**-ax with the central C p_z orbital. The **2b** orbital is formed by a combination of **3b**-br, **1b**-br, **2b**-eq, **1b**-ax, and **3b**-ax with the central C p_x and p_y orbitals. The **3a** orbital is formed by a combination of **6a**-br, **4a**-br, **5a**-eq, **4a**-ax, and **5a**-ax. The **3b** orbital is formed by a combination of **5b**-br, **4b**-eq, and **4b**-ax. The HOMO of $Ru_6C(CO)_{17}$ (**4a**) has mainly **4a**-eq character, which is a Ru−Ru metal−metal bond, and a small amount of **5a**-br character. The LUMO of $Ru_6C(CO)_{17}$ (**5a**) is mainly a combination of **5a**-br and **5a**-ax character with a small amount of **4a**-eq character.

Combining the $Ru_6C(CO)_{17}$ unit and two $Pd(PR_3)$ fragments to complete the assembly of the cluster yields a donor−acceptor description for these principal bonding interactions. The two $Pd(PR_3)$ acceptor orbitals combine to form two nearly degenerate orbitals, the LUMO (**b**) and LUMO+1 (**a**) of the $[Pd(PR_3)]_2$ unit. These two orbitals accept electrons from the **3b** and **3a** of the $Ru_6C(CO)_{17}$ unit (see Scheme 13 and Figure 7).

An analysis of the overlap populations both among the fragments and between individual metal atoms suggests that (1) there is strong Ru−C bonding between the six Ru and the central C atom of the octahedron; (2) there is direct Ru−Ru bonding

Scheme 8

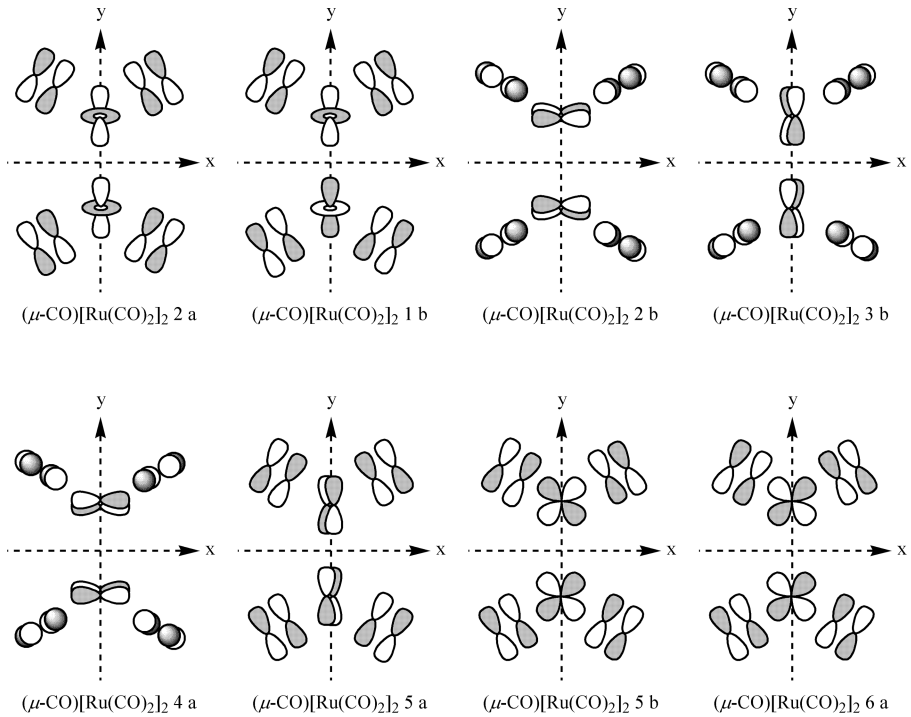

Scheme 9

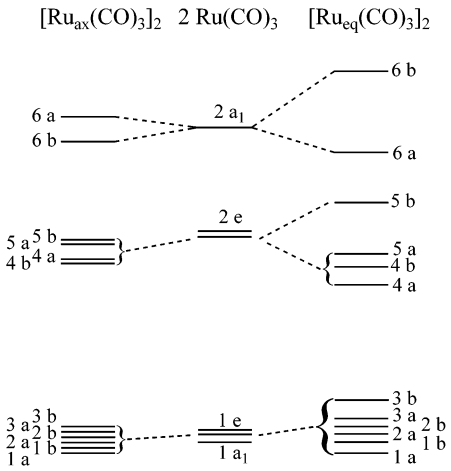

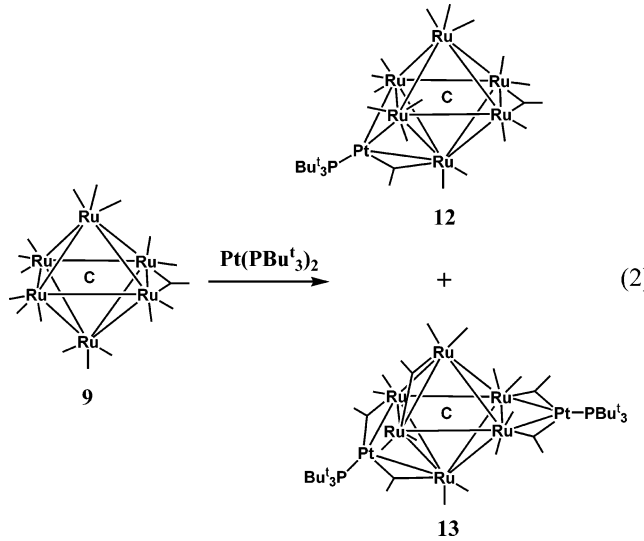

between adjacent Ru, except for the two Ru of the (μ-CO)-[Ru$_{br}$(CO)$_2$]$_2$ unit, which do not have a direct Ru−Ru bond because of the symmetrically bridging CO[28] and where the strongest Ru−Ru interaction is between the two Ru$_{eq}$ that are opposite the two-carbonyl-bridged Ru (of the (μ-CO)[Ru$_{br}$-(CO)$_2$]$_2$ unit); and (3) there are direct Ru−Pd interactions as well as strong Ru−C(O)−Pd bonding where the direct metal−metal bonds are supported by "linear" semibridging CO's.[27] Thus, the single-best valence representation, which is constructed from both the orbital and overlap population analysis, is shown in Scheme 14 (terminal CO's not represented), where the lines indicate significant bonding but not necessarily a classical 2c/2e− bond.

Pt(PBu$^t_3$)$_2$ reacts similarly with **9** to yield the diplatinum complex Ru$_6$(CO)$_{17}$(μ_6-C)[Pt(PBu$^t_3$)]$_2$, **13**, in 24% yield; in addition a monoplatinum complex, Ru$_6$(CO)$_{17}$(μ_6-C)[Pt(PBu$^t_3$)], **12**, was also obtained in 11% yield, eq 2.

Both compounds were characterized by IR, ^{1}H- and ^{31}P NMR and single-crystal X-ray diffraction analyses. Selected bond distances and angles for compounds **12** and **13** are given in Tables 6 and 7, respectively. Compound **12** consists of an Ru$_6$ octahedron with a carbon atom in the center. The Pt(PBu$^t_3$) group is bonded to three ruthenium atoms, forming a cap on the Ru(2)−Ru(3)−Ru(6) triangle, see Figure 8. Once again there was no loss of CO from **9**, and thus the compound can be viewed as a mono-Pt(PBu$^t_3$) adduct of Ru$_6$(CO)$_{17}$(μ_6-C). The Ru−Pt bond distances to the triply bridging Pt(PBu$^t_3$) group lie in the range 2.8834(9)−2.9314(6) Å and are similar to those found in the triply bridging isomer of **11**: 2.8050(6)−3.0531(6) Å.

Like compound **11**, compound **13** also has two independent molecules in the asymmetric unit in its crystal structure. However, in this case both molecules are structurally similar with two Pt(PBu$^t_3$) groups bridging two Ru−Ru bonds, making

Scheme 10

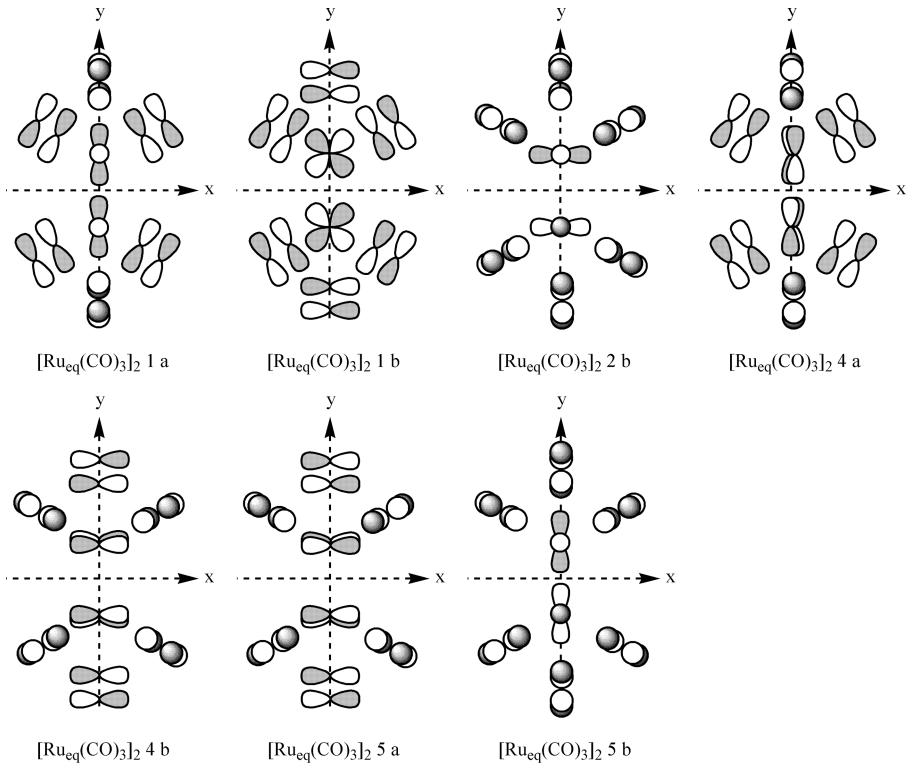

Scheme 11

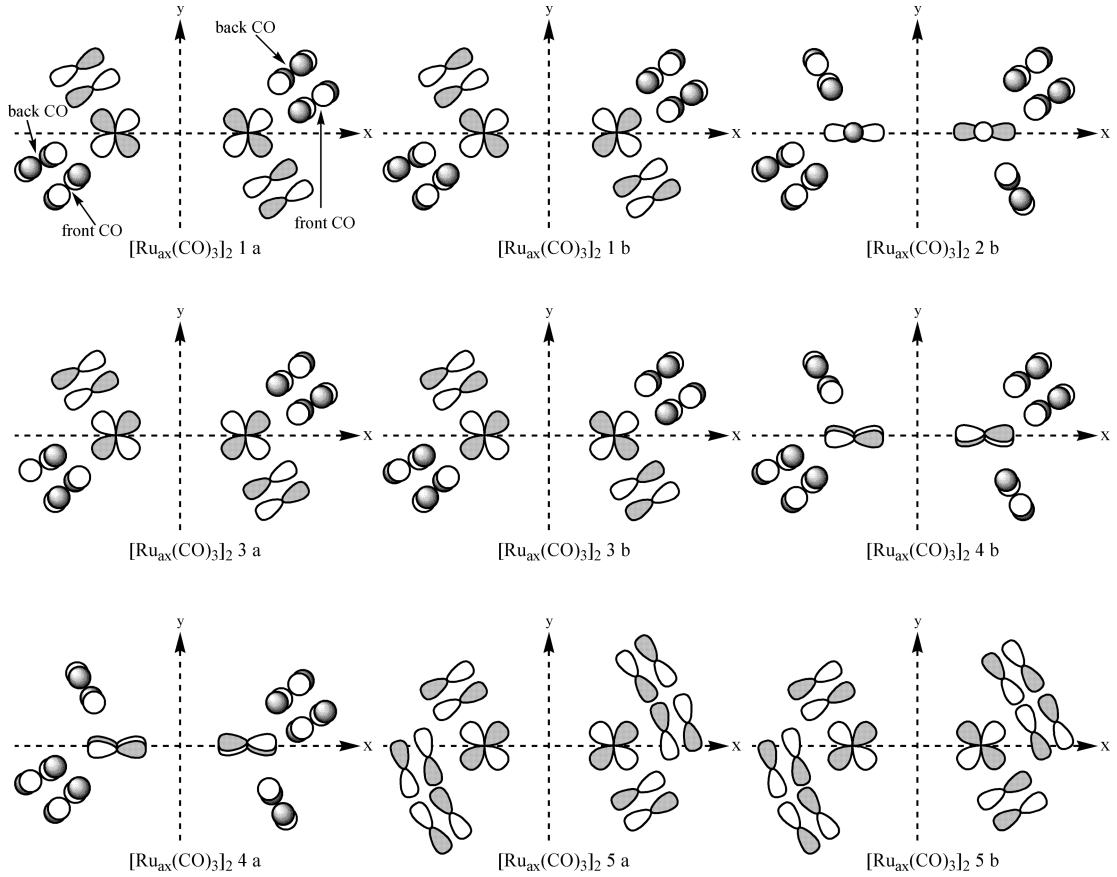

Scheme 12

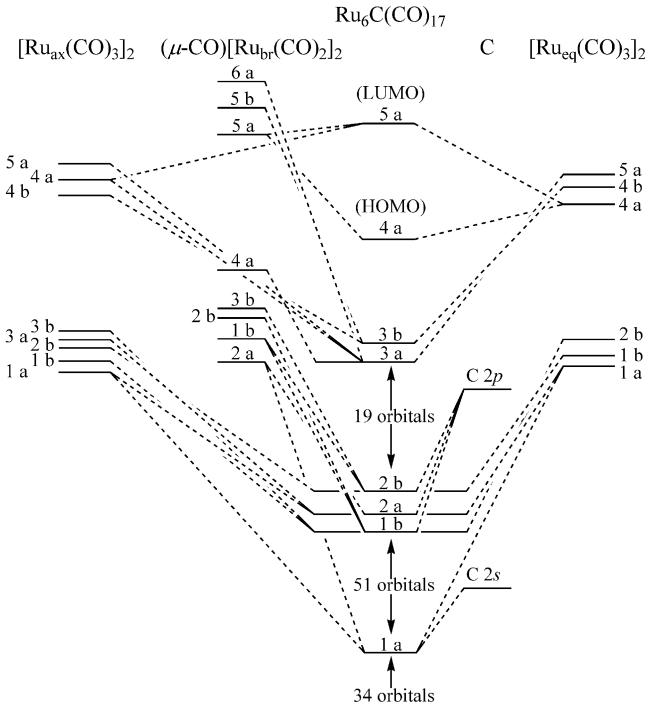

them analogous to the isomer of **11** which has Pd(PBu$^t_3$) groups bridging two Ru−Ru bonds, see Figure 9. Each Pt−Ru bond has a bridging CO ligand. The molecule has C_2 symmetry, with the two-fold axis running through the Ru(1)−Ru(4)−Ru(6)−Ru(2) plane and the bridging CO ligand on Ru(1) and Ru(4). The Pt−Ru distances lie in the range 2.7498(8)−2.8727(8) Å and are similar to the Pd−Ru distances found in **11**: 2.7790(6)−2.8423(6) Å.

The reaction of the benzene-coordinated Ru$_6$ carbonyl cluster, Ru$_6$(CO)$_{14}$(η^6-C$_6$H$_6$)(μ_6-C), **14**, with Pd(PBu$^t_3$)$_2$ at room temperature yielded mono- and dipalladium complexes Ru$_6$(CO)$_{14}$(η^6-C$_6$H$_6$)(μ_6-C)[Pd(PBu$^t_3$)]$_n$ where $n = 1$ (**15**), $n = 2$ (**16**), eq 3.

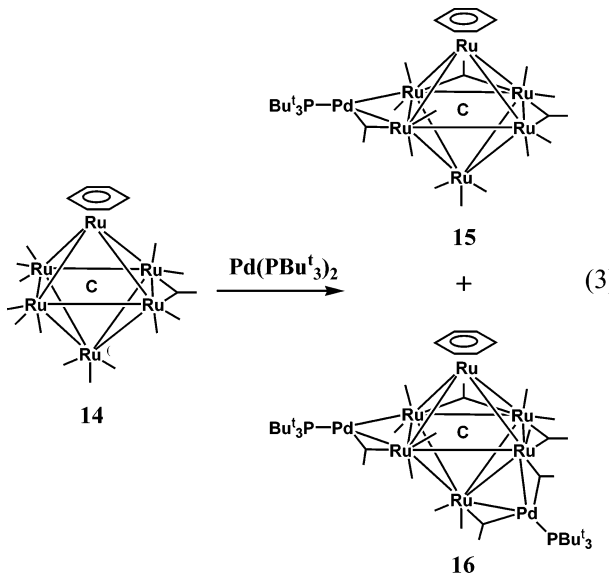

Both compounds were characterized by IR, ^{1}H- and ^{31}P NMR and single-crystal X-ray diffraction analyses. Selected bond distances and angles for compounds **15** and **16** are given in

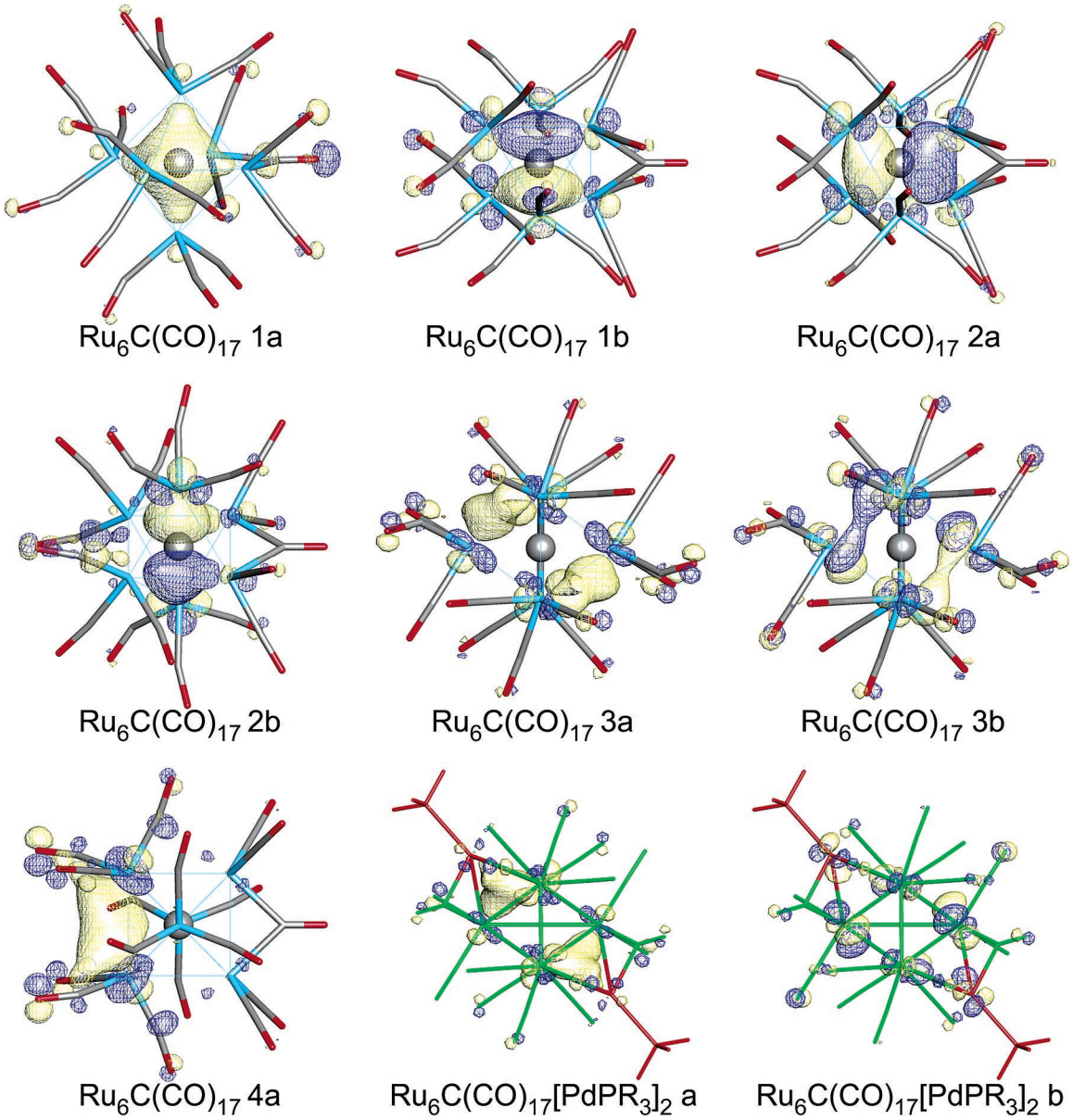

Figure 7. Seven orbitals important to cluster bonding for the core $Ru_6C(CO)_{17}$ unit (**1a**, **1b**, **2a**, **2b**, **3a**, **3b**, and **4a** as labeled in Scheme 12) and the two main orbitals of the $Ru_6C(CO)_{17}(PdPR_3)_2$ cluster responsible for two $PdPR_3$ fragments bonding to the $Ru_6C(CO)_{17}$ unit (**b** and **a** as labeled in Scheme 13).

Scheme 13

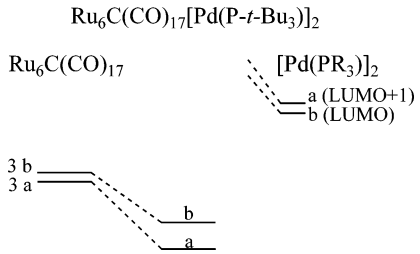

Tables 8 and 9, respectively. An ORTEP diagram of the molecular structure of **15** is shown in Figure 10. Compound **15** consists of an Ru_6 octahedron with a carbon atom in the center, a benzene ligand coordinated to one of the ruthenium atoms, Ru(1), and a $Pd(PBu^t_3)$ group bridging the Ru(2)−Ru(3) bond. Here once again, there was no loss of CO from the Ru_6 starting material, and thus compound **15** can be viewed as a mono-Pd-(PBu^t_3) adduct of $Ru_6(CO)_{14}(\eta^6\text{-}C_6H_6)(\mu_6\text{-}C)$. A bridging CO ligand from Ru(2) to the palladium atom helps stabilize this interaction. The Ru(2)−Pd(1) and Ru(3)−Pd(1) bond distances are 2.7929(9) and 2.8210(9) Å, respectively, and are similar to the Ru−Pd and Ru−Pt distances found in compounds **11**, **12**, and **13**.

Scheme 14

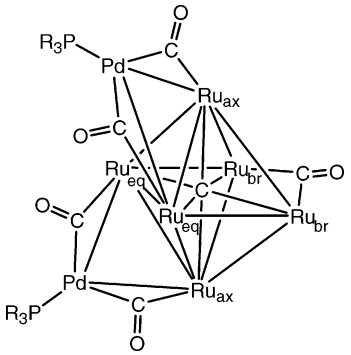

Table 6. Selected Intramolecular Distances and Angles for $Ru_6(CO)_{17}(\mu_6\text{-}C)[Pt(PBu^t_3)]$, **12**[a]

(a) Distances

atom	atom	distance (Å)	atom	atom	distance (Å)
Pt(1)	P(1)	2.3401(18)	Ru(3)	Ru(6)	2.8648(11)
Pt(1)	Ru(2)	2.8834(9)	Ru(4)	Ru(5)	2.7819(7)
Pt(1)	Ru(3)	2.8927(9)	Ru(4)	Ru(6)	3.0239(10)
Pt(1)	Ru(6)	2.9314(6)	Ru(5)	Ru(6)	3.0161(10)
Ru(1)	Ru(2)	3.8346(11)	Ru(1)	C(1)	2.057(5)
Ru(1)	Ru(3)	2.8466(11)	Ru(2)	C(1)	2.047(11)
Ru(1)	Ru(4)	2.9659(11)	Ru(3)	C(1)	2.065(10)
Ru(1)	Ru(5)	2.9546(11)	Ru(4)	C(1)	2.104(10)
Ru(2)	Ru(3)	3.1968(7)	Ru(5)	C(1)	2.085(9)
Ru(2)	Ru(5)	2.8652(13)	Ru(6)	C(1)	2.041(5)
Ru(2)	Ru(6)	2.8594(11)	O(av)	C(av)	1.14(1)
Ru(3)	Ru(4)	2.8650(13)			

(b) Angles

atom	atom	atom	angle (deg)	atom	atom	atom	angle (deg)
Ru(2)	Pt(1)	Ru(3)	67.209(16)	Ru(1)	Ru(3)	Ru(6)	91.53(3)
Ru(2)	Pt(1)	Ru(6)	58.90(2)	Ru(1)	C(1)	Ru(6)	173.6(3)
Ru(3)	Pt(1)	Ru(6)	58.93(2)	Ru(3)	C(1)	Ru(5)	169.9(5)
Ru(1)	Ru(2)	Ru(6)	91.89(3)				

[a] Estimated standard deviations in the least significant figure are given in parentheses.

Table 7. Selected Intramolecular Distances and Angles for $Ru_6(CO)_{17}(\mu_6\text{-}C)[Pt(PBu^t_3)]_2$, **13**[a]

(a) Distances

atom	atom	distance (Å)	atom	atom	distance (Å)
Pt(1)	P(1)	2.340(3)	Ru(2)	Ru(3)	2.9785(10)
Pt(1)	Ru(2)	2.7726(9)	Ru(2)	Ru(5)	2.8688(11)
Pt(1)	Ru(3)	2.8291(8)	Ru(2)	Ru(6)	2.8859(10)
Pt(2)	P(2)	2.355(3)	Ru(3)	Ru(4)	2.859711)
Pt(2)	Ru(5)	2.8727(8)	Ru(3)	Ru(6)	2.8540(11)
Pt(2)	Ru(6)	2.7674(8)	Ru(4)	Ru(5)	2.9587(10)
Pt(3)	P(3)	2.335(3)	Ru(4)	Ru(6)	2.9554(10)
Pt(3)	Ru(8)	2.8326(8)	Ru(5)	Ru(6)	2.9573(9)
Pt(3)	Ru(9)	2.7723(8)	Ru(1)	C(1)	2.090(8)
Pt(4)	P(4)	2.347(3)	Ru(2)	C(1)	2.051(8)
Pt(4)	Ru(10)	2.8715(8)	Ru(3)	C(1)	2.065(8)
Pt(4)	Ru(12)	2.7494(8)	Ru(4)	C(1)	2.067(8)
Ru(1)	Ru(2)	2.9614(10)	Ru(5)	C(1)	2.068(8)
Ru(1)	Ru(3)	2.975710)	Ru(6)	C(1)	2.021(8)
Ru(1)	Ru(4)	2.8305(11)	O(av)	C(av)	1.15(1)
Ru(1)	Ru(5)	2.8688(11)			

(b) Angles

atom	atom	atom	angle (deg)	atom	atom	atom	angle (deg)
Ru(2)	Pt(1)	Ru(3)	64.23(2)	Ru(1)	Ru(2)	Ru(6)	89.31(3)
Ru(5)	Pt(2)	Ru(6)	63.21(2)	Ru(1)	Ru(3)	Ru(6)	89.64(3)
Ru(8)	Pt(3)	Ru(9)	64.22(2)	Ru(1)	C(1)	Ru(6)	178.4(4)
Ru(10)	Pt(4)	Ru(12)	63.51(2)	Ru(3)	C(1)	Ru(5)	178.4(4)

[a] Estimated standard deviations in the least significant figure are given in parentheses.

An ORTEP diagram of the molecular structure of **16** is shown in Figure 11. Compound **16** consists of an Ru_6 octahedron with a carbon atom in the center, a benzene ligand coordinated to one of the ruthenium atoms, Ru(1), and two $Pd(PBu^t_3)$ bridging groups. Again there was no loss of CO from the starting material. Like compound **15**, the dipalladium adduct of $Ru_6(CO)_{14}(\eta^6\text{-}C_6H_6)(\mu_6\text{-}C)$, **16**, has one $Pd(PBu^t_3)$ group bridging the Ru(2)−Ru(3) bond with a CO ligand bridging the Ru(2)−Pd(1) bond, but it also has a second $Pd(PBu^t_3)$ group bridging

(27) One (bridging) CO contributes 2 e⁻, two $Ru(CO)_2$ fragments contribute 0 e⁻ each, four $Ru(CO)_3$ fragments contribute 2 e⁻ each, one C contributes 4 e⁻, and two $Pd(PR_3)$ fragments contribute 0 e⁻ each for a total of 14 e⁻ (or 7 e⁻ pairs) which provides for seven cluster bonds and a bi-capped octahedral structure. Hall, M. B. In *Metal−Metal Bonds and Clusters in Chemistry and Catalysis*; Fackler, J. P., Jr., Ed.; Plenum Press: New York: 1990; p 265.

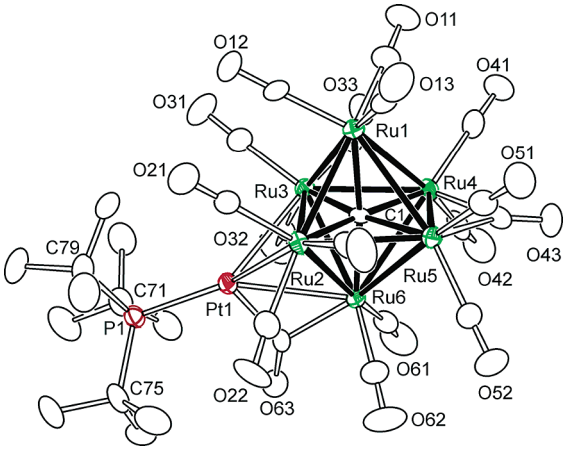

Figure 8. ORTEP diagram of the molecular structure of $Ru_6(CO)_{17}(\mu_6\text{-}C)[Pt(PBu^t_3)]$, **12**, showing thermal ellipsoids at 30% probability.

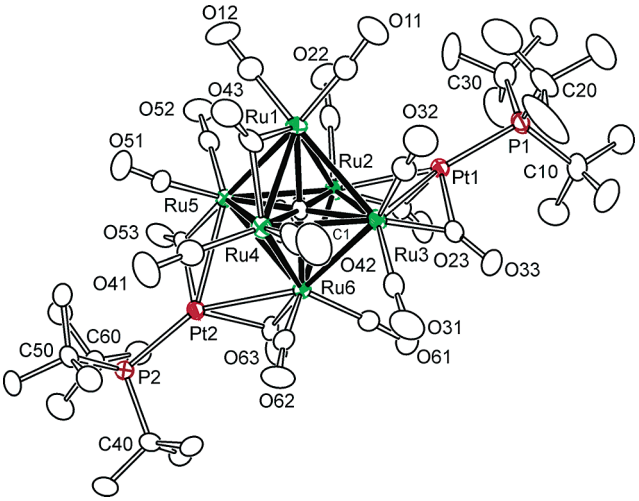

Figure 9. ORTEP diagram of the molecular structure of $Ru_6(CO)_{17}(\mu_6\text{-}C)[Pt(PBu^t_3)]_2$, **13**, showing thermal ellipsoids at 30% probability.

Table 8. Selected Intramolecular Distances and Angles for $Ru_6(CO)_{14}(\eta^6\text{-}C_6H_6)(\mu_6\text{-}C)[Pd(PBu^t_3)]$, **15**[a]

(a) Distances

atom	atom	distance (Å)	atom	atom	distance (Å)
Pd(1)	P(1)	2.392(2)	Ru(3)	Ru(6)	2.8726(9)
Pd(1)	Ru(2)	2.7929(9)	Ru(4)	Ru(5)	2.8274(9)
Pd(1)	Ru(3)	2.8210(9)	Ru(4)	Ru(6)	2.9547(9)
Ru(1)	Ru(2)	2.8409(9)	Ru(5)	Ru(6)	2.9110(10)
Ru(1)	Ru(3)	2.8548(9)	Ru(1)	C(1)	1.928(7)
Ru(1)	Ru(4)	2.8759(9)	Ru(2)	C(1)	2.037(7)
Ru(1)	Ru(5)	2.8776(9)	Ru(3)	C(1)	2.078(7)
Ru(2)	Ru(6)	2.8755(9)	Ru(4)	C(1)	2.119(7)
Ru(2)	Ru(5)	2.9653(9)	Ru(5)	C(1)	2.060(7)
Ru(2)	Ru(3)	3.0650(9)	Ru(6)	C(1)	2.079(7)
Ru(3)	Ru(4)	2.8532(9)			

(b) Angles

atom	atom	atom	angle (deg)	atom	atom	atom	angle (deg)
Ru(2)	Pd(1)	Ru(3)	66.18	Ru(1)	C(1)	Ru(6)	178.3(4)
Ru(1)	Ru(2)	Ru(6)	88.99(2)	Ru(3)	C(1)	Ru(5)	170.3(4)
Ru(1)	Ru(3)	Ru(6)	88.78(3)				

[a] Estimated standard deviations in the least significant figure are given in parentheses.

Table 9. Selected Intramolecular Distances and Angles for $Ru_6(CO)_{14}(\eta^6\text{-}C_6H_6)(\mu_6\text{-}C)[Pd(PBu^t_3)]_2$, **16**[a]

(a) Distances

atom	atom	distance (Å)	atom	atom	distance (Å)
Pd(1)	P(1)	2.4030(18)	Ru(2)	Ru(3)	3.0698(7)
Pd(1)	Ru(2)	2.8275(7)	Ru(3)	Ru(4)	2.8546(8)
Pd(1)	Ru(3)	2.8052(8)	Ru(3)	Ru(6)	2.8678(8)
Pd(2)	P(2)	2.431(2)	Ru(4)	Ru(5)	2.8075(8)
Pd(2)	Ru(2)	3.1947(8)	Ru(4)	Ru(6)	2.9835(8)
Pd(2)	Ru(5)	2.8047(8)	Ru(5)	Ru(6)	2.9529(8)
Pd(2)	Ru(6)	2.8639(8)	Ru(1)	C(1)	1.936(6)
Ru(1)	Ru(2)	2.8292(8)	Ru(2)	C(1)	2.053(6)
Ru(1)	Ru(3)	2.8447(7)	Ru(3)	C(1)	2.071(6)
Ru(1)	Ru(4)	2.8450(8)	Ru(4)	C(1)	2.114(6)
Ru(1)	Ru(5)	2.8451(8)	Ru(5)	C(1)	2.064(6)
Ru(2)	Ru(6)	2.9014(7)	Ru(6)	C(1)	2.066(6)
Ru(2)	Ru(5)	2.9941(8)			

(b) Angles

atom	atom	atom	angle (deg)	atom	atom	atom	angle (deg)
Ru(2)	Pd(1)	Ru(3)	66.047(19)	Ru(1)	Ru(3)	Ru(6)	88.95(2)
Ru(5)	Pd(2)	Ru(6)	62.78(2)	Ru(1)	C(1)	Ru(6)	178.1(3)
Ru(1)	Ru(2)	Ru(6)	88.59(2)	Ru(3)	C(1)	Ru(5)	170.4(3)

[a] Estimated standard deviations in the least significant figure are given in parentheses.

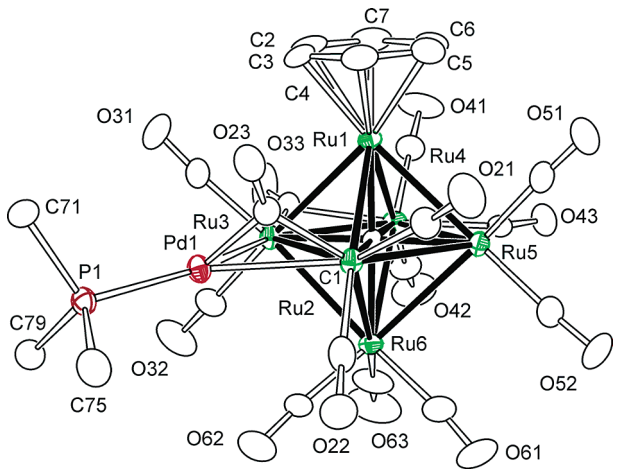

Figure 10. ORTEP diagram of the molecular structure of $Ru_6(CO)_{14}(\eta^6\text{-}C_6H_6)(\mu_6\text{-}C)[Pd(PBu^t_3)]$, **15**, showing thermal ellipsoids at 30% probability. The methyl groups have been omitted for clarity.

the Ru(5)−Ru(6) bond. Both the Ru(5)−Pd(2) and Ru(6)−Pd(2) bonds have a bridging CO ligand. The Ru−Pd bond distances lie in the range 2.8047(8)−2.8639(8) Å and are similar to the Ru−Pd and Ru−Pt bond distances found in compounds **11**, **12**, **13**, and **15**. In the solid-state structure of **16** the two PBu^t_3 ligands are inequivalent, and so one would expect to see the two respective resonances in its ^{31}P NMR spectrum. However, the ^{31}P NMR spectrum of **16** shows only a single resonance even at −80 °C. Although it is possible that the molecule has adopted a different structure in solution having

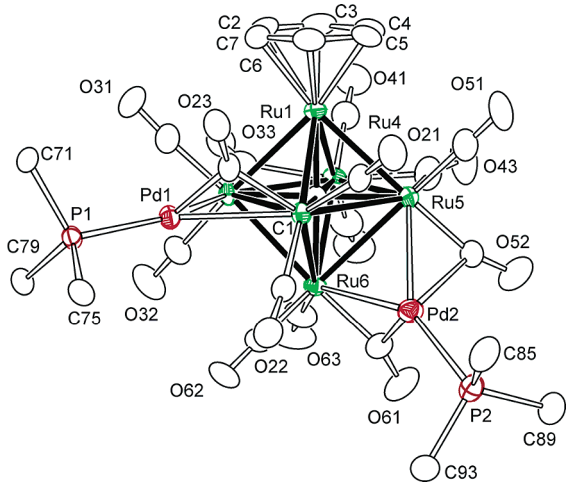

Figure 11. ORTEP diagram of the molecular structure of $Ru_6(CO)_{14}(\eta^6\text{-}C_6H_6)(\mu_6\text{-}C)[Pd(PBu^t_3)]_2$, **16**, showing thermal ellipsoids at 30% probability. The methyl groups have been omitted for clarity.

equivalent PBu^t_3 groups, it is also possible that the molecule is dynamically active on the NMR time scale and the $Pd(PBu^t_3)$ groups are interchanging equivalent sites rapidly on the NMR time scale. We have recently shown that both $Pt(PBu^t_3)$ and $Pd(PBu^t_3)$ groups can migrate rapidly about the $Ru_5(CO)_{15}(C)$ cluster.[13b,c]

One can envision the description of the bonding interactions for compounds **12**, **13**, **15**, and **16** to be similar also to that of **11**, as in **11** the other compounds all contain an Ru_6 octahedron with $M(PBu^t_3)$ groups (M = Pd or Pt) and bridging CO ligands to help stabilize the interactions between the ruthenium atoms and the $M(PBu^t_3)$ groups.

Mixed-metal clusters containing ML groups, M = Cu, Ag, or Au coordinated by phosphine ligands (L = PR_3) may have similar bonding schemes when the atom M is bonded to only two additional metal atoms.[29] For example, the cationic group $[Au(PR_3)]^+$ has only 12 e^- and is isoelectronic to the $[M(PR_3)]$ (M = Ni, Pd or Pt) group. The $[Au(PR_3)]^+$ group has also been shown to adopt both edge-bridging and triple-bridging bonding to triangular metal groups.[30]

Although there have been major efforts to prepare bimetallic cluster complexes containing palladium[31,32] and platinum[32,33] in recent years, to date very few palladium−ruthenium complexes have been formed, and the reaction of $[Pd(\eta\text{-}C_4Ph_4)(Me_2CO)_2]^{2+}$ with the ruthenium anions $[Ru_5(CO)_{14}(\mu_6\text{-}C)]^{2-}$ and $[Ru_6(CO)_{17}(\mu_6\text{-}C)]^{2-}$ yielded only ruthenium compounds containing the $\eta\text{-}C_4Ph_4$ ligand formed by ligand transfer.[34] We have

(28) Simpson, C. Q.; Hall, M. B. *J. Am. Chem. Soc.* **1992**, *114*, 1641. It is well-known that symmetrically bridging carbonyl ligands reduce the direct M−M bonding because the C lone pair destabilizes the direct M−M σ bond, while the CO π^* stabilizes the M−M π^* orbital. On the other hand, linear semibridging carbonyl ligands use their π^* to stabilize the M−M σ bond.

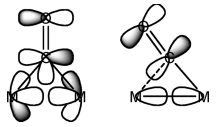

(29) Salter, I. D. Vol. Ed. In *Comprehensive Organometallic Chemistry II*; Abel, E. W., Stone, F. G. A., Wilkinson, G., Eds.; Pergamon: Oxford, 1995, vol 10, p 225.
(30) (a) Bunkhall, S. R.; Holden, D.; Johnson, B. F. G.; Lewis, J.; Pain, G. N.; Raithby, P. R.; Taylor, M. J. *Chem Commun.* **1984**, 25. (b) Henrick, K.; Johnson, B. F. G.; Lewis, J.; Mace, J.; McPartin, M.; Morris, J. *Chem Commun.* **1985**, 1617. (c) Lavigne, G.; Papageorgiou, F.; Bonnet, J. J. *Inorg. Chem.* **1984**, *23*, 609.
(31) (a) Lee, S.-M.; Wong, W.-T. *J. Cluster Sci.***1998**, *9*, 417. (b) Nakajima, T.; Ishiguro, A.; Wakatsuki, Y. *Angew. Chem. Int. Ed.* **2000**, *39*, 1131. (c) Brivio, E.; Della Pergola, R.; Garlaschelli, L.; Demartin, F.; Manassero, M.; Sansoni, M.; Zanello, P.; Laschi, F.; Heaton, B. T. *J. Chem. Soc., Dalton Trans.* **1994**, 3237.
(32) Kuwata, S.; Mizobe, Y.; Hidai, M. *J. Am. Chem. Soc.* **1993**, *115*, 8499.
(33) (a) Farrugia, L. J. *Adv. Organomet. Chem.* **1990**, *31*, 301. (b) Pignolet, L. H.; Aubart, M. A.; Craighead, K. L.; Gould, R. A. T.; Krogstad, D. A.; Wiley, J. S. *Coord. Chem. Rev.* **1995**, *143*, 219. (c) Xiao, J. L.; Puddephatt, R. J. *Coord. Chem. Rev.* **1995**, *143*, 457.
(34) Dyson, P. J.; Ingham, S. L.; Johnson, B. F. G.; McGrady, J. E.; Mingos, D. M. P.; Blake, A. J. *J. Chem. Soc., Dalton Trans.* **1995**, 2749.

now demonstrated that the bis-phosphine compounds $M(PBu^t_3)_2$, M = Pd and Pt, are excellent reagents for the transfer of Pd- and $PtPBu^t_3$ groups to ruthenium cluster compounds under mild conditions to produce a variety of new bimetallic complexes containing palladium and platinum.[13] These compounds should be useful precursors for the preparation of bimetallic nanoparticles[1−8] for new applications in catalysis.[9,10]

Acknowledgment. This research was supported by the Office of Basic Energy Sciences of the U.S. Department of Energy under Grant No. DE-FG02-00ER14980. We thank Strem for donation of a sample of $Pt(PBu^t_3)_2$. The work at TAMU was supported by the NSF (CHE98-00184), The Welch Foundation (A-0648), and Texas A&M University.

Supporting Information Available: CIF files for each of the structural analyses. This material is available free of charge via the Internet at http://pubs.acs.org.

JA039541P